PHYSICAL REVIEW D **82,** 014510 (2010)

Infrared dynamics of minimal walking technicolor

Luigi Del Debbio,[1,*] Biagio Lucini,[2,†] Agostino Patella,[2,‡] Claudio Pica,[3,§] and Antonio Rago[4,‖]

[1]*SUPA, School of Physics and Astronomy, University of Edinburgh, Edinburgh EH9 3JZ, Scotland, United Kingdom*
[2]*School of Physical Sciences, Swansea University, Singleton Park, Swansea SA2 8PP, United Kingdom*
[3]*CP-Origins, University of Southern Denmark, Odense, 5230 M, Denmark*
[4]*Department of Physics, Bergische Universität Wuppertal, Gaussstrasse 20, D-42119 Wuppertal, Germany*

(Received 20 April 2010; published 29 July 2010)

We study the gauge sector of minimal walking technicolor, which is an $SU(2)$ gauge theory with $n_f = 2$ flavors of Wilson fermions in the adjoint representation. Numerical simulations are performed on lattices $N_t \times N_s^3$, with N_s ranging from 8 to 16 and $N_t = 2N_s$, at fixed $\beta = 2.25$, and varying the fermion bare mass m_0, so that our numerical results cover the full range of fermion masses from the quenched region to the chiral limit. We present results for the string tension and the glueball spectrum. A comparison of mesonic and gluonic observables leads to the conclusion that the infrared dynamics is given by an $SU(2)$ pure Yang-Mills theory with a typical energy scale for the spectrum sliding to zero with the fermion mass. The typical mesonic mass scale is proportional to and much larger than this gluonic scale. Our findings are compatible with a scenario in which the massless theory is conformal in the infrared. An analysis of the scaling of the string tension with the fermion mass toward the massless limit allows us to extract the chiral condensate anomalous dimension γ_*, which is found to be $\gamma_* = 0.22 \pm 0.06$.

DOI: 10.1103/PhysRevD.82.014510 PACS numbers: 11.15.Ha, 12.60.Nz, 12.39.Mk, 12.39.Pn

I. INTRODUCTION

A possible mechanism of electroweak symmetry breaking is provided by strongly interacting dynamics beyond the standard model (BSM) [1,2]. In this picture, a new strongly coupled gauge interaction acting at energy scales of the order of 1 TeV is conjectured. This interaction embeds the standard model gauge group $SU(2)_L \otimes U(1)_Y$ and contains fermionic degrees of freedom (different from the standard model fermions) that do not interact directly with the latter. The chiral symmetry of the BSM interaction breaks spontaneously at the scale of 1 TeV. This breaking provides mass to the Z and $W^{\pm}$ bosons of the standard model. Historically, this framework is known as technicolor; the new bosons are referred to as technibosons and the new fermions as technifermions. In order to give mass to the standard model fermions, another new gauge interaction acting at higher energy scales (*extended technicolor*) is introduced.

In the original proposals the strongly interacting BSM dynamics was obtained by rescaling QCD. The ratio between the scale of the technicolor model and the QCD scale can then be used to determine the mass spectrum of the BSM theory. However, this scenario proves to be inadequate to provide a mechanism of mass generation for fermions without running into problems with flavor changing neutral currents. A more refined framework that could avoid those problems is walking technicolor [3–6].

Walking theories are realized as deformations of theories with an infrared (IR) fixed point, i.e. a point in which the β functions for the couplings of the theory vanish [7,8]. The role played in this scenario by the fermion representation has been emphasized in Refs. [9,10]. In particular, for theories in the two-index symmetric and adjoint representations, an IR fixed point can be reached at smaller values of the number of fermion flavors n_f than for theories involving fundamental fermions.

Like any other BSM framework, technicolor has to confront the stringent experimental bounds for new physics summarized in the S and T parameters [11]. Recent reviews of the phenomenological aspects of technicolor theories can be found in Refs. [12–16]. It is currently an open question whether a theoretically consistent framework for electroweak symmetry breaking can be drawn from those ideas. In particular, one would like to explore from first principles whether $SU(N)$ gauge theories with n_f fermion flavors in the fundamental or in a two-index representation can provide a viable walking scenario for some values of N and n_f. Such theories would be natural candidates as models of strongly interacting BSM dynamics, which eventually will be tested at the LHC.

Ultimately, the issue of determining the features of a $SU(N)$ gauge theory coupled with n_f fermion flavors transforming according to some representation $\mathcal{R}$ of the gauge group is of a nonperturbative nature, and as such it can be studied in the framework of lattice gauge theories (see e.g. [17] for a complementary approach based on AdS/CFT techniques). Following the work of Ref. [18], other lattice studies have focused on theories with fermions in two-index representations conjectured to be relevant as models of strongly interacting BSM dynamics: preliminary results

*luigi.del.debbio@ed.ac.uk
†b.lucini@swansea.ac.uk
‡a.patella@swansea.ac.uk
§pica@cp3.sdu.dk
‖rago@physik.uni-wuppertal.de

have appeared for $SU(2)$ with two fermions in the adjoint representation [19–23], and $SU(3)$ with two fermions in the symmetric representation [24]. These studies found a mass spectrum characterized by the degeneracy of the pseudoscalar (PS) and the vector meson in a wide range of fermion masses. Complementary investigations of the running of the coupling [25–30], and of the exponents that govern the scaling toward the massless limit [31–34] found preliminary indication for the existence of an infrared fixed point. Note that while in $SU(2)$ with adjoint fermions there seems to be a consensus that the theory has an infrared-conformal fixed point, for $SU(3)$ with sextet fermions the study of Ref. [35] supports a QCD-like scenario, while Refs. [36,37] favor a walking scenario. A closely related line of research is the lattice determination of the critical number of flavors for the onset of the conformal window in the $SU(3)$ gauge theory with fermions in the fundamental representation [38–49]. Reference [50] provides a perturbative determination of renormalization constants relating lattice and continuum observables in $SU(N)$ gauge theories with fermions in two-index representations. A recent account of the activity in the field is provided in Refs. [34,51,52]. For current numerical studies of conformal gauge theories, it proves to be helpful to have analytical estimates of the extent of the conformal window; recent works on this subject are reported in Refs. [53–56].

Numerical simulations of the spectrum of candidate theories of electroweak symmetry breaking beyond the standard model have focused almost exclusively on the meson spectrum (and, in particular, on the states that in QCD are the lowest-lying particles of the meson isovector spectrum, namely, the pseudoscalar and the vector mesons). Recently, investigating the case of a $SU(2)$ gauge theory with two fermion flavors in the adjoint representation (which is commonly referred to as *minimal walking technicolor*), we have pointed out in Ref. [57] that a clean signature of conformality in the chiral limit can be obtained by comparing mesonic and gluonic observables. In particular, a conformal gauge theory broken with a small fermion mass term displays the phenomenon of *hyperscaling* and *locking*, i.e. all the ratios of spectral quantities are independent of the fermion mass if the latter is sufficiently small. This paper has the twofold motivation of discussing more extensively the general expectations for the spectrum when a small mass term breaks explicitly conformal invariance, and of presenting the details of our analysis of the data in the gluonic sector leading to the conclusions of Ref. [57] about the likely existence of an infrared fixed point, having increased the statistics at some values of the lattice parameters. This work complements the investigation reported in Ref. [58], where our results for mesonic observables were discussed. We shall use the evidence found for the theory to have an infrared fixed point to perform a scaling analysis of our observables as a function of the fermion mass and provide an estimate for the anomalous dimension of the condensate, whose value has relevant phenomenological implications.

As in Refs. [57,58], the study reported here is at fixed lattice spacing. One key issue that should be carefully discussed is whether our results are relevant for the continuum physics. In general, the program of extracting the values of observables in the continuum from lattice simulations of BSM models is still at an early stage; in practice, numerical results are obtained for volumes and lattice couplings that are argued to be good approximations of the continuum system. Assessing the reliability of lattice simulations for continuum physics requires then a detailed knowledge of the phase structure of the lattice theory. More in detail, it is easy to prove analytically that deep in the strong coupling phase a $SU(N)$ lattice pure gauge theory is always confined. This feature survives when fermions with sufficiently high mass are added to the action. The lattice strong coupling, also known as the bulk phase, is separated from the continuum phase by either a phase transition or a smooth crossover (for a study of the strong coupling regime with fermions in the two-index representation, see [59]). Note that the latter phase may or may not be confining. In order to obtain a reliable continuum extrapolation, only points for which the system is in the same phase as the continuum theory must be considered. Hence, one of the preliminary tasks of lattice simulations is to identify the exact extent of the bulk phase. This program has been carried out in Refs. [19–21], which have shown that the bulk phase roughly corresponds to lattice couplings $\beta \leq 2.0$. However, staying clear from the bulk phase could not be a sufficient condition for getting relevant results for the real-world physics: another aspect that needs to be considered is the physical size of the volume, which should be such that analytical predictions for finite-size corrections could be reliably used to extract information from the data. Although at first sight this issue could seem more under control than the one related to lattice artifacts, this is a prejudice modeled after our understanding of QCD. If the physics of our system is conformal, QCD does not provide a reliable guidance for analyzing the numerical results. In fact, recent analytical and numerical arguments have shown that, even in the continuum, the theory in a finite box is characterized by a nontrivial phase structure in terms of the lattice volume and of the fermion mass [60–62]. The finite-volume phases are characterized by different behaviors of the order parameter related to confinement, the trace of the Polyakov loop. In order to check for possible lattice artifacts, we measured the Polyakov loop wrapping around the spatial directions. We find that the bare fermion mass can significantly affect the phase structure at fixed lattice size. In particular, at fixed volume, when lowering the bare fermion mass the system goes from the infinite-volume confined phase (as shown by the presence of a nonzero string tension) to a spatially deconfined regime. We find that gluonic observables are strongly affected by this

change of regime, while mesonic quantities behave smoothly across it. This could be an effect of the separation at finite mass of the confinement and the chiral symmetry breaking scales in theories with adjoint fermions (observed in Refs. [63,64]), which would be an expected feature for a candidate model of technicolor that has a large-distance dynamics different from the QCD one.

This work is organized as follows. Section II discusses the hyperscaling and locking phenomena, which arises when an infrared-conformal gauge theory is deformed with a small mass term. In Sec. III we define the discretized theory and set the notations. Results for the phase structure, the string tension extracted via Polyakov loop correlators, the string tension extracted from expectation values of Wilson loops, and glueball masses are reported in Secs. IV, V, VI, and VII. A comparison between the dynamical and the quenched simulations performed keeping the string tension and the pseudoscalar mass fixed at the values dictated by the dynamical theory is then provided, and from this comparison hyperscaling and locking are shown to take place in the model studied in this work (Sec. VIII). Section IX illustrates our scaling analysis aimed to determine the chiral condensate anomalous dimension γ_*. Finally, Sec. X reports our conclusions and possible future directions of our work.

II. MASS-DEFORMED INFRARED-CONFORMAL GAUGE THEORIES

For technical reasons which depend on the specific fermion discretization, lattice simulations can only be performed with a nonvanishing mass term for the fermions. In particular Wilson fermions break chiral symmetry explicitly even for vanishing bare mass, so that the massless limit is only obtained by fine-tuning the parameters in the Lagrangian. Moreover, it is impossible to simulate at arbitrarily small masses if the lattice spacing and the volume are kept constant, since small eigenvalues of the Dirac operator are generated, the simulation algorithm becomes unstable and unphysical phases can appear. The extrapolation from a region of small enough masses (but still in a safe region of parameters) to the chiral limit can be performed only under the guidance of an analytical picture.

For QCD-like theories, chiral perturbation theory (in the infinite volume, in the epsilon and delta regimes) allows one to extrapolate physical quantities from a region of small enough masses to the chiral limit.

The natural question is what should we expect if we deform an IR-conformal theory with a small mass term, and how do we recover the chiral limit? Hence, before illustrating the details of our simulations, we set the frame for the picture in the latter case.

A. Renormalization group analysis

A gauge theory with massless fermions (in the continuum) depends on a single parameter, the running coupling $g(\mu_0)$ at some reference scale μ_0, or alternatively the renormalization group (RG)-invariant parameter Λ. This is valid for both confining and IR-conformal theories. In confining theories the particle masses (except the Goldstone bosons) are proportional to the parameter Λ in the chiral limit. In the case of IR-conformal theories, where the spectrum is made of unparticles, Λ is not associated to particle masses, but sets the energy scale at which the crossover between the asymptotically free and conformal regimes occurs. An explicit definition of Λ is not relevant for our discussion and will then be omitted.

When the IR-conformal theory is deformed by a mass term for the fermions, a particle spectrum with a mass gap is expected to be generated. The theory depends now on one more parameter, the running mass $m(\mu_0)$ at the reference scale μ_0; alternatively, an RG-invariant parameter M can be suitably defined. Close enough to the chiral limit (in the *scaling region*), the particle masses are expected to be independent of Λ. We will see that under a regularity hypothesis, those masses are expected to be proportional to M. This result is standard in the statistical-mechanics analysis of second-order phase transitions, but it will be presented here using the language of quantum field theory.

The running of the renormalized mass is computed by solving the RG equation (in a mass-independent renormalization scheme):

$$\mu \frac{dm}{d\mu}(\mu) = -\gamma(g(\mu))m(\mu), \tag{1}$$

which yields

$$\begin{aligned} m(\mu) &= m(\mu_0)\exp\left\{-\int_{g(\mu_0)}^{g(\mu)} \frac{\gamma(z)}{\beta(z)} dz\right\} \\ &\equiv Z_m(\mu, \mu_0, \Lambda) m(\mu_0). \end{aligned} \tag{2}$$

As we are going to show, the function $Z_m(\mu, \mu_0, \Lambda)$ can be rewritten in a more convenient form. The theory we are interested in is asymptotically free in the UV. The β and γ functions close to the UV fixed point are

$$g \to 0: \ \beta(g) \simeq -\beta_0 g^3, \tag{3}$$

$$\gamma(g) \simeq \gamma_0 g^2, \tag{4}$$

where the lowest order coefficients come from a one-loop computation [T_R and $C_2(R)$ are the generator normalization and the Casimir of the fermionic representation]:

$$\beta_0 = \frac{1}{(4\pi)^2}\left(\frac{11}{3}N - \frac{4}{3}T_R n_F\right), \tag{5}$$

$$\gamma_0 = \frac{6C_2(R)}{(4\pi)^2}. \tag{6}$$

From now on, we will be interested only in the IR-conformal scenario. Close to the IR fixed point we assume a regular behavior for the RG functions:

$$g \to g_*: \beta(g) \simeq \beta_*(g - g_*), \tag{7}$$

$$\gamma(g) \simeq \gamma_*, \tag{8}$$

where β_* and γ_*, which are scheme-independent quantities, are in general not accessible by a perturbative expansion.

Integrating the RG equation $\mu dg/d\mu = \beta(g)$ close to the fixed points, the asymptotic running-coupling behavior is derived:

$$\mu \to \infty: g(\mu) \simeq \frac{1}{2\beta_0 \log(\mu/\Lambda)}, \tag{9}$$

$$\mu \to 0: g(\mu) \simeq g_* - A_g\left(\frac{\mu}{\Lambda}\right)^{\beta_*}. \tag{10}$$

We separate now the singular behaviors close to the fixed points in the multiplicative renormalization function of the mass:

$$Z_m(\mu, \mu_0, \Lambda) = \exp\left\{-\int_{g(\mu_0)}^{g(\mu)}\left(\frac{\gamma(z)}{\beta(z)} - \frac{\gamma_*}{\beta_*(z-g_*)} + \frac{\gamma_0}{\beta_0 z}\right)dz\right\}\exp\left\{-\int_{g(\mu_0)}^{g(\mu)}\frac{\gamma_*}{\beta_*(z-g_*)}dz\right\}\exp\left\{\int_{g(\mu_0)}^{g(\mu)}\frac{\gamma_0}{\beta_0 z}dz\right\} = \frac{\tilde{Z}_m(\mu/\Lambda)}{\tilde{Z}_m(\mu_0/\Lambda)}, \tag{11}$$

where the function

$$\tilde{Z}_m(\mu/\Lambda) = [g_* - g(\mu)]^{-(\gamma_*/\beta_*)} g(\mu)^{\gamma_0/\beta_0} \times \exp\left\{\int_{g(\mu)}^{g_*}\left(\frac{\gamma(z)}{\beta(z)} - \frac{\gamma_*}{\beta_*(z-g_*)} + \frac{\gamma_0}{\beta_0 z}\right)dz\right\} \tag{12}$$

is defined in such a way that the integral in the exponential is finite both for $\mu \to 0$ and $\mu \to \infty$.

An RG-invariant fermionic mass M can be defined by means of the condition $m(M) = M$. Plugging Eq. (11) in Eq. (2), and choosing $\mu_0 = M$ we get the relationship:

$$\tilde{Z}_m(\mu/\Lambda)^{-1} m(\mu) = \tilde{Z}_m(M/\Lambda)^{-1} M. \tag{13}$$

If the RG-invariant mass M is much larger than Λ, the following asymptotic behavior can be easily shown to hold by using the previous relationship:

$$m(\mu) = A_\infty \tilde{Z}_m(\mu/\Lambda) M\left[\log\frac{M}{\Lambda}\right]^{\gamma_0/\beta_0}. \tag{14}$$

At fixed energy scale μ, the running mass diverges as M goes to infinity. The fermions decouple and the theory is effectively described by a pure Yang-Mills (YM) theory with a scale $\Lambda_{\rm YM} \simeq \Lambda$. At leading order in Λ/M, the parameter M coincides with the quark pole mass. In fact, if $S(p)$ is the quark propagator in a fixed gauge, the perturbative expansion yields

$$S(p)^{-1} = \left[1 + \sum_{n=1}^{\infty} A_n\left(\frac{-p^2}{\mu^2}, \frac{m(\mu)}{\mu}\right) g^{2n}(\mu)\right] \times \left[\not{p} - m(\mu) - \sum_{n=1}^{\infty} B_n\left(\frac{-p^2}{\mu^2}, \frac{m(\mu)}{\mu}\right) g^{2n}(\mu)\right], \tag{15}$$

where the pole mass $\bar{m}$ is defined in such a way that the quark propagator has a pole for $-p^2 = \bar{m}^2$. The pole mass is RG invariant; therefore it can be computed for an arbitrary value of μ. It is convenient to choose $\mu = M$:

$$\bar{m} = M + \sum_{n=1}^{\infty} B_n\left(\frac{\bar{m}^2}{M^2}, 1\right) g^{2n}(M). \tag{16}$$

At large masses $M \gg \Lambda$, the terms in the sum are suppressed since the running coupling goes to zero, and $\bar{m} \simeq M$. In this regime, the meson masses are just twice the quark pole mass, while the glueball masses are the same as in the pure Yang-Mills theory:

$$M_{\rm mes} = 2M; \tag{17}$$

$$M_{\rm glue} = B_{\rm glue}\Lambda. \tag{18}$$

On the other hand, the chiral limit is reached for values of M much smaller than Λ. In this case, Eq. (13) becomes

$$m(\mu) = A_0 \tilde{Z}(\mu/\Lambda)\Lambda^{-\gamma_*} M^{1+\gamma_*}, \tag{19}$$

producing the power law that is characteristic of the IR fixed point deformed with a small fermionic mass.

Consider now a physical mass M_X in a channel X (it can be the mass of a particle or other physical quantities like the square root of the string tension). As every observable, this will be a function of the renormalized coupling $g(\mu)$, the mass $m(\mu)$, and the subtraction scale μ. However a physical quantity must be RG invariant:

$$M_X[\mu, g(\mu), m(\mu)] = M_X \tag{20}$$

for every value of μ. The RG equation for M_X has a simple solution in terms of the RG-invariant quantities Λ and M:

$$M_X = M F_X(M/\Lambda), \tag{21}$$

where F_X is a generic function of the ratio M/Λ. In particular, if $F_X(x) = \alpha/x$, we get $M_X = \alpha\Lambda$ which is an RG-invariant quantity, but does not vanish in the chiral limit.

The *hyperscaling hypothesis*, which is assumed in the standard discussion of second-order phase transitions (see

e.g. Ref. [65]), asserts the regularity of masses (or correlation lengths in the language of statistical mechanics) with respect to the irrelevant couplings. Consider Eq. (20) for $\mu = M \ll \Lambda$:

$$\begin{aligned} M_X &\simeq M_X[M, g_* - A_g(M/\Lambda)^{\beta_*}, M] \\ &= M_X[1, g_* - A_g(M/\Lambda)^{\beta_*}, 1]M \\ &\simeq M_X[1, g_*, 1]M \equiv A_X M, \end{aligned} \tag{22}$$

where we used dimensional analysis for the second line, and regularity with respect to g in the last one. Under the hyperscaling hypothesis, RG-invariant IR quantities depend only on M (and not on Λ) close enough to the chiral limit. The hyperscaling hypothesis constrains the F_X function defined in Eq. (21) to be regular in the chiral limit:

$$\lim_{x\to 0} F_X(x) = A_X. \tag{23}$$

Since a mass gap is expected to be generated at nonzero values of M, A_X must be different from zero.

Combining Eqs. (19) and (22) we get the power law for physical masses close to the chiral limit:

$$\begin{aligned} M_X &= A_X M \\ &= A_X[A_0 \tilde{Z}(\mu/\Lambda)]^{-1/(1+\gamma_*)} \Lambda^{\gamma_*/(1+\gamma_*)} m(\mu)^{1/(1+\gamma_*)}. \end{aligned} \tag{24}$$

We remind one that this expression is valid for every value of μ as long as $M \ll \Lambda$. In particular, the independence of M_X of Λ is manifest at values $\mu \ll \Lambda$:

$$M_X = A_X \mu^{\gamma_*/1+\gamma_*} m(\mu)^{1/1+\gamma_*}. \tag{25}$$

If we interpret the RG in the Wilsonian sense and choose $\mu = a^{-1}$ to be the cutoff, Eq. (24) yields the power law dependence of physical masses on the bare quark mass $aM_X \propto (am_0)^{1/1+\gamma_*}$.

B. Scaling region and locking scale

Under the hyperscaling hypothesis, the function F_X defined in Eq. (21) is expected to approach a nonzero value A_X in the chiral limit. We can define the scaling region for a given channel X as the range of $x = M/\Lambda$ around $x = 0$, where the function $F_X(x)$ deviates from its asymptotic behavior by a small relative amount ϵ:

$$\left| \frac{F_X(x) - A_X}{A_X} \right| < \epsilon. \tag{26}$$

In the scaling region, the mass M_X obeys the power law (24) as a function of the running mass up to corrections of order ϵ. The extension of the scaling region will depend on the size of the discarded subleading contributions to formula (24) in the chosen channel.

Consider now the square root of the fundamental string tension $M_\sigma = \sqrt{\sigma}$ (which is well defined for dynamical fermions in the adjoint representation) and the lightest isovector meson (which is always the pseudoscalar one), with mass $M_{\rm PS}$. A finite value $x = \bar{x}$ exists, below which both these channels are in the scaling region. This means that below the mass $M_{\rm lock} = \bar{x}\Lambda$, the corrections to the hyperscaling behavior of M_σ and $M_{\rm PS}$ masses are relatively smaller than ϵ. Also the ratio $M_{\rm PS}/M_\sigma$ for every fermionic mass below $M_{\rm lock}$ will be very similar to its asymptotic value $A_{\rm PS}/A_\sigma$:

$$\left| \frac{M_{\rm PS}}{M_\sigma} - \frac{A_{\rm PS}}{A_\sigma} \right| < O(\epsilon). \tag{27}$$

The dynamics is dramatically different below and above the mass $M_{\rm lock}$. In the large-mass region, $M \gg \Lambda$, the gluonic and mesonic masses are parametrically independent. All the gluonic masses are proportional to Λ, while all the mesonic masses are equal to $2M$:

$$M_{\rm PS} = 2M, \tag{28}$$

$$M_\sigma = B_\sigma \Lambda. \tag{29}$$

The ratio $M_{\rm PS}/M_\sigma$ goes to infinity in the large-mass limit. For masses below $M_{\rm lock}$ the two masses $M_{\rm PS}$ and M_σ enter the scaling region, becoming both independent of Λ and proportional to M. The ratio $M_{\rm PS}/M_\sigma$ is locked to its asymptotic value $A_{\rm PS}/A_\sigma$. We will refer to $M_{\rm lock}$ as the locking mass.

The behavior of the masses in between the large-mass and scaling regions and the actual value of $\bar{x}$ depend on the details of the dynamics. However if the dynamics is such that the locking occurs at a value $\bar{x} = M_{\rm lock}/\Lambda \gg 1$, then both M_σ and $M_{\rm PS}$ at the locking scale are still approximately the same as in the large-mass region:

$$B_\sigma \simeq \frac{M_\sigma(M = M_{\rm lock})}{\Lambda} \simeq \frac{A_\sigma M_{\rm lock}}{\Lambda} = A_\sigma \bar{x}, \tag{30}$$

$$A_{\rm PS} \simeq 2, \tag{31}$$

and the ratio $M_{\rm PS}/M_\sigma$ is locked at a very large value:

$$\frac{A_{\rm PS}}{A_\sigma} \simeq \frac{2\bar{x}}{B_\sigma} \gg 1. \tag{32}$$

Mesons are much heavier than the square root of the string tension for every value of M. Choosing an intermediate energy scale E such that $M_\sigma \ll E \ll M_{\rm PS}$, the effective theory describing the gluonic degrees of freedom at energies below E is a pure Yang-Mills plus power-suppressed corrections coming from the propagation of heavy quarks in the loops. In order to write the effective Lagrangian in this regime, we need all the gauge-invariant scalar operators of dimension 6 that are invariant under parity, and charge conjugation. These can be written as linear combinations of the following independent operators (a similar analysis on the lattice was carried on in Ref. [66]):

$$S_1 = \sum_{\mu,\nu,\rho} \mathrm{tr}(J_{\mu\nu\rho} J^{\mu\nu\rho}), \tag{33}$$

$$S_2 = \sum_{\mu,\nu,\rho} \mathrm{tr}(J^{\mu}{}_{\mu\rho} J_{\nu}{}^{\nu\rho}), \tag{34}$$

$$S_3 = \sum_{\mu,\nu,\rho} \mathrm{tr}(J_{\mu\nu\rho} J^{\nu\mu\rho}), \tag{35}$$

where $J_{\mu\nu\rho} = \partial_\mu F_{\nu\rho} - i[A_\mu, F_{\nu\rho}]$. Thus the effective Lagrangian can be written as

$$\mathcal{L}_{\mathrm{eff}} = -\frac{1}{2g^2}\,\mathrm{tr}(F_{\mu\nu}F^{\mu\nu}) + \sum_{i=1,2,3} \frac{a_i}{M^2} S_i + O(M^{-4}). \tag{36}$$

The scale Λ_{YM} of this low-energy pure Yang-Mills theory is in general a function of Λ and M and can be computed by matching the square root of the string tension of the low-energy effective theory with the same quantity computed in the dynamical theory:

$$B_\sigma \Lambda_{\mathrm{YM}} \left[1 + O\left(\frac{\Lambda_{\mathrm{YM}}}{M}\right)^2\right] = M_\sigma = M F_\sigma(M/\Lambda), \tag{37}$$

which implies that trivially $\Lambda_{\mathrm{YM}} \simeq \Lambda$ for $M \gg \Lambda$, while for $M < M_{\mathrm{lock}}$ then

$$\Lambda_{\mathrm{YM}} \simeq \frac{M_\sigma}{B_\sigma} \simeq \frac{A_\sigma M}{B_\sigma} \simeq \frac{M}{\bar{x}}. \tag{38}$$

In the scaling region the scale Λ_{YM} of the low-energy pure Yang-Mills theory *slides* with the RG-invariant fermionic mass M.

A comment is mandatory at this point. *At fixed value of the fermionic mass*, the low-lying spectrum of a mass-deformed IR-conformal theory with $\bar{x} \gg 1$ cannot be distinguished by the low-lying spectrum of a confining theory with heavy quarks, since they both are described by the same effective Lagrangian (36). However in a genuine heavy-quark phase the low-energy spectrum is almost independent of the mass M, while the sliding of the low-energy scale described in Eq. (38) and (equivalently) the locking of the gluonic spectrum to the mass M are ultimately a very clean signature of IR conformality.

Summarizing:

(i) We define the locking mass M_{lock} as the mass below which both the lowest isovector meson and the string tension are approximately in the chiral scaling region.

(ii) The value of $\bar{x} = M_{\mathrm{lock}}/\Lambda$ is determined by the detailed dynamics of the theory. If $\bar{x} \gg 1$ then the mesons are always much heavier than the square root of the string tension. The low-energy effective theory is a pure Yang-Mills plus small corrections, with a scale Λ_{YM} which depends on both Λ and M. For $M > M_{\mathrm{lock}} \gg \Lambda$ then the fermions completely decouple and $\Lambda_{\mathrm{YM}} \simeq \Lambda$, while for $M < M_{\mathrm{lock}}$ the only effect of the fermions in the dynamical theory is to make the low-energy scale slide with the fermionic mass $\Lambda_{\mathrm{YM}} \simeq M/\bar{x}$.

(iii) The case where $\bar{x} \gg 1$ is realized if the fixed point is perturbative [67,68]. In fact, in this case

$$\bar{x} = \exp\left(\frac{1}{2\beta_0^{\mathrm{YM}} g_*^2}\right). \tag{39}$$

The described scenarios are illustrated in the sketches in Fig. 1.

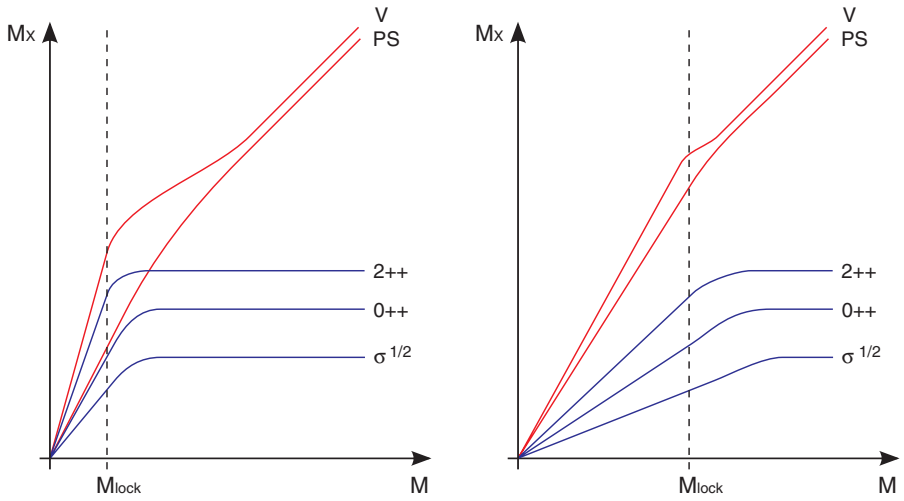

FIG. 1 (color online). Sketches of the spectrum of a mass-deformed IR-conformal theory (square root of the string tension, 0^{++} and 2^{++} glueballs, pseudoscalar and vector isovector mesons). In the left plot, the locking sets up at an intermediate value of the fermion mass, where dynamical fermion effects account for the physics of the system, but the pseudoscalar is not much lighter than the other particles in the spectrum. In the right plot, the locking sets up at a high value of the fermion mass, where the heavy-quark effective theory provides a good description of the relevant degrees of freedom. This case is realized close to the Banks-Zacks point, but is possible in principle also if a strongly coupled IR fixed point is present.

III. THE LATTICE MODEL

Consider a four-dimensional Euclidean torus $L_t \times L_s^3$, where L_t and L_s are the lengths, respectively, of the temporal and spatial directions. The space-time is discretized by introducing a lattice with spacing a, and with $N_t = L_t/a$ and $N_s = L_s/a$ sites, respectively, in the temporal and spatial directions. Lattice sites are identified by four-coordinate dimensionful vectors $x = (x_0, x_1, x_2, x_3)$. Therefore x_0/a is an integer number running from zero to $N_t - 1$, and x_i/a with $i = 1, 2, 3$ are integer numbers running from zero to $N_s - 1$. In some cases it is useful to separate the temporal coordinate from the spatial vector; we write $x = (t, \mathbf{r})$, and r is the modulus of $\mathbf{r}$. Lattice directions are indicated with a Greek symbol and run from 0 to 3. The temporal direction is chosen as the zeroth direction. We will use the same Greek symbol both for the direction index and for the vector of length a along the axis direction (the meaning of the symbol will be always clear from the context). The spatial directions are closed with periodic boundary conditions (PBC) for all fields, while the boundary conditions in the temporal direction are periodic for gauge fields and antiperiodic (ABC) for fermion fields.

The action of a $SU(N)$ gauge theory with fermions can be decomposed as

$$S = S_g + S_f, \tag{40}$$

where S_g is the discretized Yang-Mills action and S_f is the fermionic contribution. Various choices for the lattice action are possible, differing from each other by corrections that vanish in the continuum limit. At finite lattice spacing different choices are differently affected by lattice artifacts. In particular, as the lattice spacing is increased, a transition to a phase not connected with the continuum (the *bulk phase*) takes place. A careful exploration of the phases of the system on a lattice as a function of the lattice parameters is then mandatory.

For the gauge part, we use the Wilson action:

$$S_g = \beta \sum_{x,\mu<\nu} \left(1 - \frac{1}{N} \mathrm{Re\,tr} \mathcal{P}_{\mu\nu}(x)\right), \tag{41}$$

where $\mathcal{P}_{\mu\nu}(x)$ is the parallel transport of the link variable $U(x, \mu) \in SU(N)$ along the elementary square of the lattice identified by the point x and the pair of directions (μ, ν). β is related to the bare coupling g_0^2 by $\beta = 2N/g_0^2$. The value of the coupling determines the physical value of the ultraviolet cutoff, the lattice spacing a. Note that independently of the fermion representation, the link variables are in the fundamental representation of $SU(N)$.

The fermion part of the action for a spinorial field $\psi(x)$ defined on sites x and transforming in the representation R can be written as

$$S_f = a^4 \sum_{k=1}^{n_f} \bar{\psi}_k(x) D_m \psi_k(x), \tag{42}$$

where D_m is the Dirac operator, in the Wilson discretization:

$$\begin{aligned} D_m(x, y) = &\left(\frac{4}{a} + m_0\right)\delta_{x,y} \\ &- \frac{1}{2a}\sum_{\mu}\{(1 - \gamma_\mu)U^R(x, \mu)\delta_{x,y-\mu} \\ &+ (1 + \gamma_\mu)U^R(y, \mu)^\dagger \delta_{x,y+\mu}\}, \end{aligned} \tag{43}$$

where U^R are the link variables in the representation R, and m_0 is the bare mass.

The functional integral is given by

$$Z = \int (\mathcal{D}U)(\mathcal{D}\bar{\psi})(\mathcal{D}\psi) e^{-S} = \int (\mathcal{D}U)(\det D_m)^{n_f} e^{-S_g} \tag{44}$$

and the vacuum expectation value of an operator $O(U, \psi, \bar{\psi})$ by

$$\langle O \rangle = \frac{1}{Z} \int (\mathcal{D}U_\mu)(\mathcal{D}\bar{\psi})(\mathcal{D}\psi) O e^{-S}, \tag{45}$$

where once again it is possible to integrate over the fermion fields and obtain an expression that involves only an integral over the link variables. For further details on the lattice formulation, we refer to Refs. [19,58].

We performed numerical simulations for $SU(2)$ gauge theory with $n_f = 2$ Wilson fermions in the adjoint representation at a fixed value of $\beta = 2.25$, different values of the bare mass, and different lattices, the smallest one being a 16×8^3 lattice, and the largest one being 32×16^3. We used the rational hybrid Monte Carlo (RHMC) algorithm [69] as implemented in the HIREP code, which is described and benchmarked in detail in Ref. [19]. The full list of the parameters we used in our simulations can be found in Tables I, II, and III. In this work we are mainly interested in gluonic observables. For every choice of the parameters we compute:

(i) the traced Polyakov loops in every direction, in order to identify the regime of the theory, as described in Sec. IV;
(ii) the string tension by means of correlators of spatial and temporal Polyakov loops, as described in Sec. V;
(iii) the static force and potential, as described in Sec. VI;
(iv) the glueball masses, as described in Sec. VII.

We follow the convention that lattice observables are dimensionful, with the same dimension of the corresponding continuum observable. Of course we can measure only dimensionless ratios. For instance given a mass m, only the dimensionless quantity am can be extracted from lattice simulations. Determining $a(\beta)$, and ultimately the physical value m, requires one to set the physical scale using an appropriate observable. We will not perform the

TABLE I. Results for the Polyakov loop distribution and the string tension, for all the simulations on the 16×8^3 lattice. We analyzed the Polyakov loop distribution by using the number of configurations quoted in the 4th column (for the three lowest masses we could not safely discard the thermalization). In the 5th column, "S" indicates that the distribution has a single maximum in zero, "A" indicates that a double peak or an asymmetric peak is visible, and "?" indicates that we cannot clearly distinguish between the two cases. The temporal (6th column) and spatial (7th column) string tensions computed from correlators of Polyakov loops are quoted. In the 8th column, "yes" indicates that the data for the temporal and spatial string tensions have an overlap at 1σ.

			Spatial center		String tension from Polyakov correlators		
Lattice	V	$-am_0$	N_{conf}	Realization	$a\sigma_t^{1/2}$	$a\sigma_s^{1/2}$	$\sigma_s = \sigma_t$
S0	16×8^3	-0.5	8000	S	...	...	...
S1	16×8^3	-0.25	8000	S	0.4085(57)	0.393(11)	Yes
S2	16×8^3	-0	8000	S	0.3998(57)	0.388(11)	Yes
S3	16×8^3	0.25	8000	S	0.328(23)	0.358(12)	Yes
S4	16×8^3	0.5	8000	S	0.3576(46)	0.347(11)	Yes
S5	16×8^3	0.75	8000	S	0.282(13)	0.2784(75)	Yes
S6	16×8^3	0.90	8000	S	0.227(11)	0.2452(67)	Yes
A0	16×8^3	0.95	8000	S	0.1974(83)	0.2218(35)	No
A1	16×8^3	0.975	8000	?	0.2066(97)	0.2094(49)	Yes
A2	16×8^3	1	8000	?	0.1960(85)	0.2252(62)	No
A3	16×8^3	1.025	8000	A	0.1689(44)	0.2109(46)	No
A4	16×8^3	1.05	8000	A	0.1679(47)	0.2074(38)	No
A5	16×8^3	1.075	6400	A	0.1629(27)	0.20680(94)	No
A6	16×8^3	1.1	6400	A	0.1553(28)	0.20443(82)	No
A7	16×8^3	1.125	...	...	0.1462(26)	0.20423(87)	No
A8	16×8^3	1.15	...	...	0.1368(20)	0.20402(67)	No
A9	16×8^3	1.175	...	...	0.1310(19)	0.2067(11)	No

TABLE II. As Table I, for the simulations on the 24×12^3 lattice.

			Spatial center		String tension from Polyakov correlators		
Lattice	V	$-am_0$	N_{conf}	Realization	$a\sigma_t^{1/2}$	$a\sigma_s^{1/2}$	$\sigma_s = \sigma_t$
B0	24×12^3	0.95	9501	S	0.225(11)	0.2181(23)	Yes
B1	24×12^3	1	7951	S	0.1785(57)	0.1882(40)	Yes
B2	24×12^3	1.05	5620	?	0.1491(73)	0.1597(24)	Yes
B3	24×12^3	1.075	4987	A	0.1398(63)	0.1461(20)	Yes
B4	24×12^3	1.1	4194	A	0.1205(56)	0.1427(21)	No
B5	24×12^3	1.125	4001	A	0.1130(54)	0.1338(5)	No
B6	24×12^3	1.15	1500	A	0.0829(26)	0.1337(9)	No
B7	24×12^3	1.175	5001	A	0.0918(36)	0.1333(6)	No
B8	24×12^3	1.18	4490	A	0.0944(36)	0.1333(11)	No
B9	24×12^3	1.185	4335	A	0.0834(29)	0.1425(47)	No
B10	24×12^3	1.19	4336	A	0.0851(34)	0.1380(37)	No

TABLE III. As Table I, for the simulations on the 32×16^3 lattice.

			Spatial center		String tension from Polyakov correlators		
Lattice	V	$-am_0$	N_{conf}	Realization	$a\sigma_t^{1/2}$	$a\sigma_s^{1/2}$	$\sigma_s = \sigma_t$
C0	32×16^3	1.15	6145	?	0.0790(34)	0.1029(19)	No
C1	32×16^3	1.175	1871	A	0.0966(78)	0.10057(65)	Yes
C2	32×16^3	1.18	1500	A	0.0648(33)	0.1086(13)	No
C3	32×16^3	1.185	1419	A	0.0612(36)	0.09953(13)	No
C4	32×16^3	1.19	1609	A	0.0703(40)	0.1021(13)	No

step of reinstating physical units, but shall leave a (which is fixed in our case) as a parameter. However, the reader must bear in mind that knowing the value of a in terms of the quantities entering the dynamics in the continuum is important in order to confidently assess the relevance of a lattice simulation for continuum physics. For this investigation, following the detailed exploration of the phase structure of the theory performed in Ref. [21], we argue that large discretization artifacts are ruled out and we postpone to future studies a systematic investigation of these effects.

IV. CENTER SYMMETRIES AND POLYAKOV LOOPS

For a $SU(N)$ gauge theory with fermions in the adjoint representation, the action has a $\mathbb{Z}_N^4$ invariance, where each of the $\mathbb{Z}_N$ factors is associated with one direction of the system. An observable that is not invariant under the $\mathbb{Z}_N$ factor of the symmetry group associated with the direction ρ is the Polyakov loop operator in the fundamental representation wrapping around ρ:

$$\bar{P}_\rho = \sum_x{}' \prod_{n=0}^{N_\rho - 1} U(x + n\rho, \rho), \tag{46}$$

where the primed sum runs over all points of the lattice slice at $x_\rho = 0$. Consider the system in a Euclidean manifold $\mathbb{R}^3 \times S^1$, in which the direction ρ is compactified on the S^1 circle and the other three directions extend to infinity. At given radius of the S^1, the $\mathbb{Z}_N$ symmetry associated with ρ might either be a symmetry of the system or could be spontaneously broken. For simplicity, let us take ρ to be the temporal direction; the inverse radius of the S^1 has then the natural interpretation of the temperature of the system. In this case, if the system is symmetric, the trace of $\bar{P}_\rho$ is equal to zero and the system is confined at the given temperature. Conversely, a nonzero $\langle \mathrm{tr}\bar{P}_\rho \rangle$ signals the breaking of the $\mathbb{Z}_N$ symmetry associated with the direction

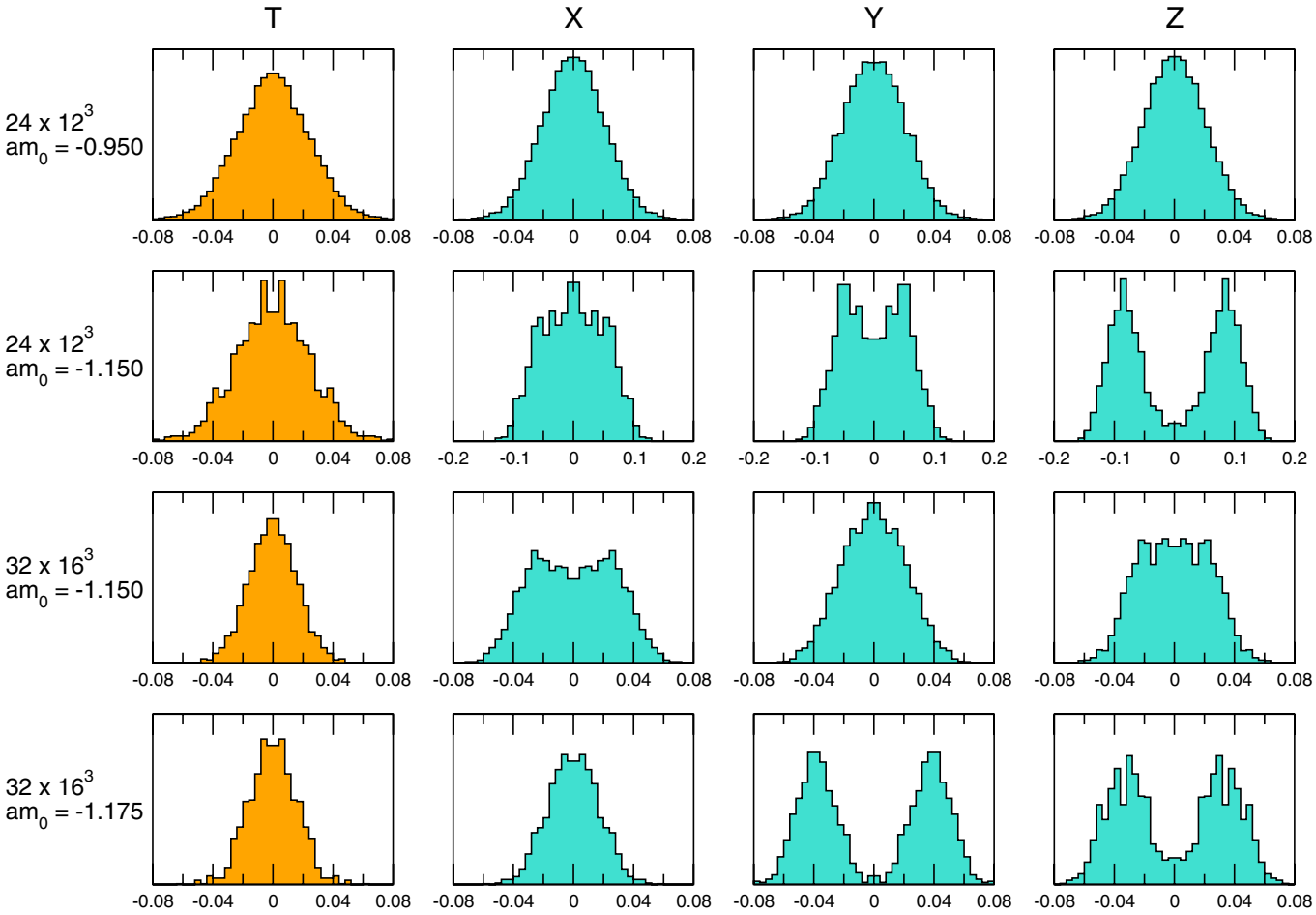

FIG. 2 (color online). Some distributions of Polyakov loops in the temporal and spatial directions. The distributions have been symmetrized by hand. At fixed volume, the distribution of the spatial Polyakov loop shows a single peak at zero at the higher mass, and it develops two peaks at the lower mass in some of the spatial directions. At fixed mass, it shows a single peak on the larger lattice, and it develops double peaks on the smaller lattice in some of the spatial directions.

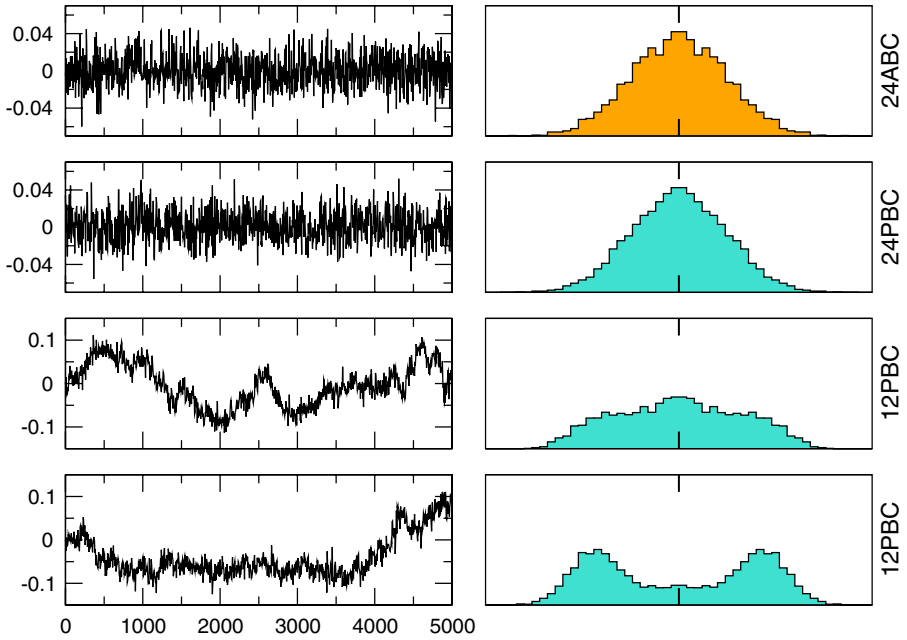

FIG. 3 (color online). Histories and distributions of Polyakov loops in the temporal (with fermionic antiperiodic boundary conditions, ABC) and spatial directions (with fermionic periodic boundary conditions, PBC), for bare mass -1.125 on the $24 \times 24 \times 12^2$ lattice. The distributions have been symmetrized by hand.

ρ and the system is deconfined. Analogously, if ρ is a spatial dimension, we call the broken phase *spatial deconfinement*.

Even if the theory is conformal in the chiral limit, a small mass drives it off the attraction basin of the IR fixed point, generating a mass gap. As for the pure gauge system, at finite temperature the theory is expected to undergo a deconfinement transition as the temporal direction is reduced down to a critical value. Because of the periodic boundary conditions for fermions in space, the reduction of a single spatial direction is more subtle. Recent numerical simulations [61] have shown that in a $SU(3)$ theory with two staggered Dirac adjoint fermions the center symmetry (which is intact at infinite volume) is first broken and then restored again as the radius of a compactified spatial direction is shrunk. The symmetry restoring transition happening when the radius is shrunk from values that set the system in the broken phase is expected from the one-loop perturbative calculation of Ref. [70]. The critical radii for the symmetry breaking and symmetry restoring transitions depend in general on the mass. Although the different discretization choice and the different gauge group might affect the phase structure, it is possible that a similar behavior characterizes $SU(2)$ with two adjoint Dirac flavors of Wilson fermions.

When the system is in a compact domain, nontrivial phases can be observed only at large N. In this case, a rich phase structure can exist, since more than one $\mathbb{Z}_N$ can be broken at the same time. For the pure gauge theory at large N, as the hypercubic volume is reduced from large values, a cascade of phase transitions takes place [71]. Each phase can be characterized by the number of the $\mathbb{Z}_N$ factors that are spontaneously broken to the trivial element of the group. The case of a large-N $SU(N)$ gauge theory with adjoint fermions on a compact domain has an even richer phase structure [72].

If the three spatial directions have a finite extension and N is finite, no phase transition can occur at any size of the system. However one can still investigate whether the distribution of the Polyakov loop in a given spatial direction has a single peak in zero (S, symmetric phase) or two separate peaks symmetric around zero (A, asymmetric phase), keeping in mind that at infinite volume the Polyakov loop distribution should display a single peak. The S phase is the finite volume and finite N equivalent of the thermodynamic phase in which the system is symmetric under the $\mathbb{Z}_N$ symmetry related to the direction wrapped by the Polyakov loop, while the A phase is the finite volume and finite N equivalent of the broken phase. We stress once again that at finite N and on a finite volume there are no distinct phases, but only different regimes. The terminology here is used only for convenience.

We measure the distributions of the Polyakov loops in all the directions. In all the lattices we consider, we always find a temporal S phase, which means that we are correctly simulating the confined thermal phase of the infinite-volume system. In lattices with geometry $N_t \times N_s^3$, we are not interested in separating the equivalent spatial di-

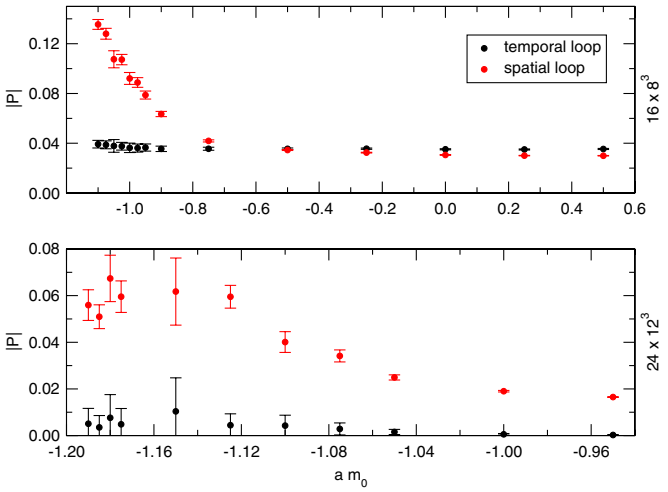

FIG. 4 (color online). Absolute value of the Polyakov loop on the 16×8^3 and 24×12^3 lattices.

rections. Hence we will say that the system is in a spatial S phase if all the spatial directions show a single peak distribution centered in zero.

For the 16×8^3 lattice, we find the spatial A phase below $am_0 \approx -0.975$. The crossover from the S phase to the A phase is very smooth. A summary of the realization of the spatial center in the 16×8^3 can be found in Table I. The two maxima of the spatial distributions are better defined on the 24×12^3 lattice, for which the spatial A phase is found below $am_0 = -1.05$ (see Table II for a summary). For the 32×16^3 lattice, all the simulated masses show distinct maxima in the distribution of the spatial Polyakov loops, except at the higher mass where we find a broad distribution with a flat region in the middle (see Table III for a summary). We show some distributions for the 24×12^3 and 32×16^3 lattices in Fig. 2. We also simulated a $24 \times 24 \times 12^2$ lattice at $am_0 = -1.125$. In this case the large spatial direction is in the S phase, while the smaller ones are in the A phase. In Fig. 3 we plot the histories and the distributions for all the Polyakov loops for the $24 \times 24 \times 12^2$ lattice.

In Fig. 4, we also report the absolute value of the Polyakov loop on the 16×8^3 and 24×12^3 lattices. As the mass is decreased, this quantity undergoes a crossover from a lower value to a higher one. This crossover moves to a noticeably lower mass when the lattice size is increasing, indicating that the A phase disappears in the large-volume limit.

The crossover from the S phase to the A phase as the spatial volume is decreased is a clear indication that at least our S phase is not in the femto-world regime, which is in the nearby of the zero-volume limit, and which is a possible source of large systematic errors in a lattice simulation [43]. Our data are actually consistent with the picture that the S phase is connected with the infinite-volume limit. However, as we shall show in detail, we still have large finite-volume effects for several of the measured observables.

V. STRING TENSION FROM CORRELATORS OF POLYAKOV LOOPS

For a $SU(N)$ gauge theory in the confined phase, a static quark-antiquark pair in the fundamental representation at large separation R is bound by the potential

$$V(R) = \sigma R, \tag{47}$$

where the string tension σ is the dynamically generated scale of the system. σ is the string tension in an effective string theory describing the low-energy dynamics of confining flux tubes connecting the quark and the antiquark. Contrary to the adjoint string tension (and to the fundamental string tension in QCD), the chromoelectric field between two fundamental sources in a gauge theory with adjoint matter is not screened. Hence, the asymptotic fundamental string tension is a well-defined quantity.

It is easy to prove analytically on the lattice that any gauge theory has a nonzero string tension at strong coupling and large fermion masses. The relevant question for the system under study is whether a region in bare parameter space exists, which is analytically connected with the continuum limit, and where the string tension is zero in the massless limit, as it should be if the theory is conformal.

The string tension can be extracted from correlators of Polyakov loops. In particular, consider the plane defined by $x_0 = 0$ and a fixed transverse coordinate in one arbitrary spatial direction (e.g. we can consider the case of constant coordinate x_1 in the first direction), and let us define

$$P_0(x_1) = \frac{1}{N_s^2} \sum_{x_2,x_3} \frac{1}{N} \mathrm{Tr}\Big(\prod_{n_0=0}^{N_t-1} U(an_0, \mathbf{r}; 0) \Big), \tag{48}$$

where $\mathbf{r}$ is the spatial vector with coordinates (x_1, x_2, x_3). For the vacuum-subtracted correlator of this quantity one finds

$$\langle P_0(x_1)^\dagger P_0(x_1 + X_1)\rangle - |\langle P_0(x_1)\rangle|^2 = \sum_{n=0}^{\infty} |c_n(L_t)|^2 e^{-E_n(L_t)X_1}, \qquad E_n > 0 \quad \forall\ n, \tag{49}$$

where the sum runs over all states $|n\rangle$ of the Hamiltonian with nonvanishing overlap $c_n = \langle 0|P_0(x_1)|n\rangle$. At large X_1 the sum is dominated by the term $|c_0(L_t)|^2 e^{-E_0(L_t)X_1}$ associated with the exponential with the lowest decay rate, $E_0(L_t)$, which is the energy of the ground state in the fundamental string sector. For a confining theory, up to subleading corrections one finds [73]

$$E_0(L_t) = \sigma L_t - c\pi(D-2)/(6L_t), \tag{50}$$

where c depends on the number of massless fermionic and bosonic modes propagating along the string and D is the dimension of the system ($D = 4$ in our case). Analogously,

if the Polyakov loop wraps a spatial direction, its vacuum-subtracted zero-momentum correlators in the temporal direction define the so-called spatial string tension. For a confined theory at zero temperature, the spatial and the temporal string tensions coincide if the system is the S phase.

In $SU(N)$ Yang-Mills theories, the effective theory describing the large-distance dynamics of the confining flux tube is a bosonic string theory [74–77]. General arguments lead to the following expansion of E_0 [78]:

$$E_0(L_t) = \sigma L_t - \frac{\pi(D-2)}{6L_t} - \frac{1}{2}\left(\frac{\pi(D-2)}{6}\right)^2 \frac{1}{\sigma L_t^3} + \sigma L_t c_6 + \cdots, \tag{51}$$

where c_6 is a term $\mathcal{O}((1/(\sigma^3 L_t^6))$. Note that Eq. (51) is the truncation to second order in $1/(\sigma L_t^2)$ of the ground state energy of a bosonic string of the Nambu-Goto type:

$$E_0(L_t) = \sigma L_t \sqrt{1 - \frac{\pi(D-2)}{3\sigma L_t^2}}. \tag{52}$$

This might suggest that the effective string theory describing the large-distance dynamics of the confining flux tube is actually of the Nambu-Goto type. These considerations do not generalize immediately to the case of dynamical fermions in the adjoint representation. In fact differently from $SU(N)$ pure Yang-Mills theory, in this case it is possible to construct explicitly fermionic open-string states. Hence, it could be that the effective theory is not bosonic, in which case the firmest result available is given by Eq. (50), with c (unknown *a priori*) counting the zero modes of the effective string. In our analysis, we will assume that the effective theory is bosonic and the string tension will be obtained from the correlator of Polyakov loops assuming Eq. (52). This assumption is justified *a posteriori* by two crucial observations: first, the string tension obtained in this way is in complete agreement with the static potentials and forces computed by Wilson loops (Sec. VI), for which no effective string theory is assumed; in addition, the low-energy dynamics will be found to be an effective Yang-Mills theory with small corrections (accordingly to the discussion in Sec. II B) for all the simulated masses, which shows that the choice of Eq. (52) is self-consistent.

For a theory that confines at zero temperature and undergoes a deconfinement phase transition at some critical temperature, the correlator in Eq. (49) still decays exponentially with the distance in the deconfined phase, provided the sources are screened; however, the inverse of the corresponding energy is now associated with a screening length, the Debye screening length. Hence, the exponential decay of Polyakov loop correlators by itself does not imply the existence of a string tension. In order to see that the theory is confining, the validity of Eq. (52) as L_t is varied needs to be proved. Alternatively, one has to show that the static potential (Sec. VI) is asymptotically linear and the slope of the linear part is related to the ground state mass extracted from Polyakov loop correlators via Eq. (52).

In general, extracting numerically the string tension from the correlator (49) proves to be technically hard, since the signal-over-noise ratio decays exponentially with the separation. A good degree of success is achieved if the zero-momentum Polyakov line is replaced by a fuzzy operator, and a reliable signal can be obtained if a variational procedure that involves different fuzzy operators is set up. There are several ways of achieving this; here we follow Refs. [79,80]. In practice, a recursive procedure is implemented, which allows one to obtain smeared links at step $l+1$ from the fuzzy links at l via the relationship

$$U^{(l+1)}(x,\mu) = \mathrm{Proj}(U^{(l)}(x,\mu) + \alpha S^{(l)}(x,\mu) + \delta D^{(l)}(x,\mu)), \tag{53}$$

where $S^{(l)}(x,\mu)$ is the sum of the four length three nonbacktracking lattice paths from x to $x + a\hat{\mu}$ (*staple*) and $D^{(l)}(x,\mu)$ is the sum of the 16 length-five nonbacktracking paths with the same start and end points (only the directions that are orthogonal to the direction in which correlations are taken enter the sums). The constants α and δ are fixed empirically in such a way that the signal is optimal. Since the (weighted) sum of the paths is not an element of the group, to obtain an object that can be interpreted as a fuzzy link this sum needs to be reprojected onto $SU(N)$; this is the meaning of the operator Proj() in Eq. (53). After k steps of smearing, consecutive pairs of smeared links going in the same direction can be multiplied to produce blocked links. The combination of smearing and blocking yields the link set $\{U^{(b)}(x,\mu)\}$ at blocking level b, which can be used to compute the fuzzy Polyakov loop operator

$$P_0^{(b)}(x) = \frac{1}{N_s^2}\sum_{y,z}\frac{1}{N}\,\mathrm{Tr}\left(\prod_{n_0=0}^{N_t/b} U^{(b)}(an_0,\mathbf{r};0)\right), \tag{54}$$

and analogously for the other directions. For sake of definiteness, we discuss the case of Polyakov loops winding in time, but similar conclusions hold for Polyakov loops wrapping around the other directions. The element bc of the correlation matrix $\tilde{C}(X_1)$ is then defined as

$$\tilde{C}_{bc}(X_1) = \langle P_0^{(b)}(x_1)^\dagger P_0^{(c)}(x_1+X_1)\rangle - \langle P_0^{(b)}(x_1)\rangle^\dagger \langle P_0^{(c)}(x_1)\rangle. \tag{55}$$

As functions of X_1, diagonal correlators involving the eigenvectors associated with the largest eigenvalues of $\tilde{C}^{-1}(0)\tilde{C}(1)$ decay as single exponentials with energies $E_0, E_1, \ldots$ already at distances of a few lattice spacings. The negligible contamination from excited states eliminates the need to go to large distances to identify the stringy state with the lowest energy; at the same time, this procedure provides an estimate of energies of excited states, associated to the single-exponential behavior of

diagonal correlators of eigenvectors corresponding to smaller eigenvalues, although the reliability of the excited spectrum depends on how large the variational basis is. The efficiency of the variational procedure is manifest in the overlap of the vacuum with the lowest-lying stringy state [i.e. the equivalent of the coefficient $|c_0|^2$ in Eq. (49)], which would be one in the ideal case in which the variational procedure identified the exact state we are interested in. In the considered fuzzying scheme, with a careful choice of the parameters α and δ it is possible to reach overlaps of the order of 0.9–0.95, which makes the contribution of excited states negligible already at distances of the order of two lattice spacings. Physically, the process of blocking and smearing allows us to build variational trial states on the scale of physical distances, while simple Polyakov loop correlators probe the physics on the scale of the lattice spacing, which is sensitive to ultraviolet fluctuations.

We remind one that we use Eq. (52) for extracting the string tension from E_0.[1] Our results for the string tension are plotted in Fig. 5. For the smearing and blocking procedures, we have used $\alpha = 0.4$ and $\delta = 0.16$. As expected, at high mass the spatial and the temporal string tensions agree and are independent of the lattice size. The signal provided by the Polyakov loop correlator is clean and the overlap $|c_0|^2$ is of order 0.9–0.95. As am_0 is reduced, on the smaller lattices the spatial and the temporal string tensions depart, and the overlap becomes of order 0.8. The disagreement between the temporal and the spatial string tensions is an indication that finite-size effects are starting to play a major role. As a matter of fact, if we simulate at fixed values of am_0 on increasingly larger lattices, we find that the spatial and the temporal string tensions eventually agree, and that they also agree with the temporal string tension of the smaller lattices. This shows that the temporal string tension is less affected by finite-size effects. This is hardly surprising, since the onset of the departure between the spatial and temporal string tension arises where the system goes from the S to the A phase. This also confirms that in the A regime strictly speaking it is not correct to talk about a spatial string tension, since the mass of the Polyakov loop is not associated with confining strings. However, for convenience we shall still use the string language. For a given volume, if the mass is lowered below the onset of spatial deconfinement, the agreement of the temporal string tension and the string tensions computed on larger volumes is lost, and the former flattens out. This kind of finite-size effects appears when the correlation length associated with the string tension becomes of the order of the spatial lattice size. In fact, for the plateau values we find $a^2\sigma_t \simeq 4N_t^{-2} = N_s^{-2}$. Taken at face value,

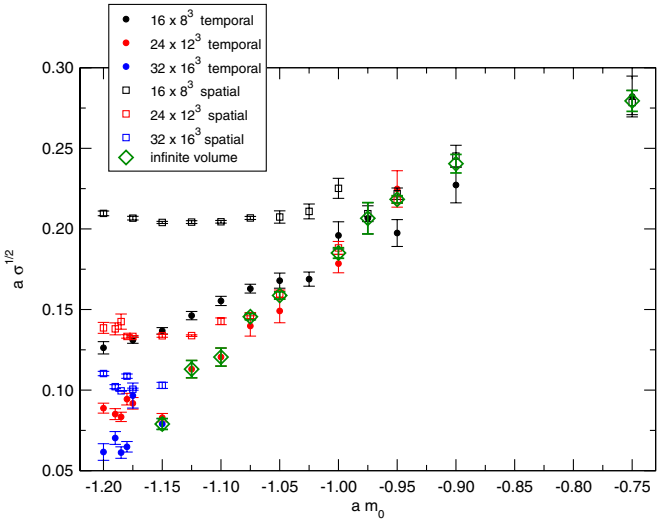

FIG. 5 (color online). Spatial and temporal string tensions at various lattice sizes as a function of am_0. Also shown is the infinite-volume estimate.

this would imply that in the thermodynamic and chiral limit $a\sqrt{\sigma_t} = 0$. However, since these results have been obtained in a phase where finite-size artifacts play a major role, a confirmation of this statement on larger lattices is necessary before we can conclude that there is no asymptotic string tension in the massless limit.

We estimate the string tension at infinite volume by choosing the determinations that are reasonably safe from finite-volume effects. Our strategy is based on the following observations. At fixed mass and in the infinite-volume limit, the temporal and spatial string tensions must coincide. At fixed volume we observe that at large enough mass, the temporal and spatial string tensions coincide. In general the spatial string tension can be determined more accurately, since correlators of shorter Polyakov loops have smaller relative errors. On the other hand, the temporal string tension is less affected by finite-volume effects and, in particular, is always well defined. Whenever the spatial and temporal string tensions agree within 1 standard deviation, we consider the weighted average of the two:

$$\sqrt{\sigma} = \frac{\frac{\sqrt{\sigma_s}}{(\Delta\sqrt{\sigma_s})^2} + \frac{\sqrt{\sigma_t}}{(\Delta\sqrt{\sigma_t})^2}}{\frac{1}{(\Delta\sqrt{\sigma_s})^2} + \frac{1}{(\Delta\sqrt{\sigma_t})^2}}, \tag{56}$$

$$\Delta\sqrt{\sigma} = \frac{1}{\sqrt{\frac{1}{(\Delta\sqrt{\sigma_s})^2} + \frac{1}{(\Delta\sqrt{\sigma_t})^2}}}. \tag{57}$$

In the A phase, where the temporal and spatial string tensions do not agree anymore, the correct string tension to be considered is the temporal one. At those values of the mass, for which more than one volume is available, the result on the largest volume has been considered.

[1] Alternatively, Eq. (51) can be used, since it gives results that are compatible well within errors with Eq. (52); on the contrary, Eq. (50) gives discrepancies of up to 20% for loops winding the spatial directions.

TABLE IV. This table shows the infinite-volume estimate for the string tension (2nd column). Where different volumes are available for the same bare mass, the larger one has been chosen. If the temporal and spatial string tensions agree within 1 standard deviation, a weighted average (w.a.) between the two has been chosen, as explained in the text. Otherwise the temporal string tension (s.t.) has been chosen. For the bare mass $am_0 = -1$, the temporal string tensions on the 16×8^3 and 24×12^3 lattices agree at the 1σ level: this suggests that for all the string tensions computed at this and higher masses on the 16×8^3 lattice, finite-volume effects are negligible. Also the temporal string tension computed on the 32×16^3 lattice at $am_0 = -1.15$ coincides at 1σ with the one computed on the 24×12^3 lattice.

$-am_0$	Inf. volume estimate of $a\sigma^{1/2}$	Method	Static potential & force
-0.25	0.4053(51)	w.a. on 16×8^3 (S1) data	$\cdots$
0	0.3976(51)	w.a. on 16×8^3 (S2) data	$\cdots$
0.25	0.352(11)	w.a. on 16×8^3 (S3) data	$\cdots$
0.5	0.3561(42)	w.a. on 16×8^3 (S4) data	$\cdots$
0.75	0.2794(63)	w.a. on 16×8^3 (S5) data	$\cdots$
0.9	0.2405(58)	w.a. on 16×8^3 (S6) data	$\cdots$
0.95	0.2184(23)	w.a. on 24×12^3 (B0) data	24×12^3
0.975	0.2066(97)	Temporal s.t. on 16×8^3 (A1)	$\cdots$
1	0.1851(33)	w.a. on 24×12^3 (B1) data	24×12^3
1.05	0.1587(23)	w.a. on 24×12^3 (B2) data	24×12^3
1.075	0.1455(19)	w.a. on 24×12^3 (B3) data	24×12^3
1.1	0.1205(56)	Temporal s.t. on 24×12^3 (B4)	24×12^3
1.125	0.1130(54)	Temporal s.t. on 24×12^3 (B5)	$24 \times 24 \times 12^3$
1.15	0.0790(34)	Temporal s.t. on 32×16^3 (C0)	32×16^3

More in detail, at the mass $am_0 = -1$ both the 24×12^3 and 16×8^3 lattices are available, and the two temporal string tensions (plus the spatial string tension on the larger volume) are in agreement at the 1σ level. For this mass and larger ones we therefore expect that the temporal string tension, as determined on the 24×12^3 and 16×8^3 lattices, is affected by smaller finite-volume effects than the statistical indetermination. In particular, the string tensions on the 24×12^3 lattice at masses $am_0 = -1$ and -0.95, and on the 16×8^3 lattice at masses $am_0 = -0.975, -0.9, -0.75, -0.5, -0.25, 0, 0.25$ are good estimates for the infinite-volume limit.

Moreover, at the mass $am_0 = -1.15$ both the 32×16^3 and 24×12^3 lattices are available, and the two temporal string tensions agree at the 1σ level. Repeating the argument above, the string tensions on the 32×16^3 lattice at mass $am_0 = -1.15$, and on the 24×12^3 lattice at masses $am_0 = -1.125, -1.1, -1.075, -1.05$ are good estimates of the infinite-volume limit. Below mass $am_0 = -1.15$ we have no control on the finite-volume effects, so we just discarded those points.

The choices described above, and the results for the estimate of the string tension at infinite volume are summarized in Table IV. All the measured string tensions and the infinite-volume estimates are also plotted in Fig. 5.

VI. STATIC FORCE AND POTENTIAL FROM WILSON LOOPS

A different way to compute the string tension is via the expectation values of Wilson loops. The advantage of this method is that it can show whether the mass extracted via Polyakov loop correlators is in fact related to the existence of an asymptotic string tension at fixed lattice geometry. As we will see, the disadvantage is that the numerical results for the string tension extracted from Wilson loops generally have larger statistical errors.

We consider the generic off-axis Wilson loop $W(T, \mathbf{R})$, describing a quark-antiquark pair separated by a spatial distance $\mathbf{R} = (X, Y, Z)$ and propagating in a straight line in the temporal direction. It will be useful to schematically decompose the close parallel transport in its spatial $U_s[t; \mathbf{r} \to \mathbf{r} + \mathbf{R}]$ and temporal $U_t[t \to t + T; \mathbf{r}]$ components:

$$W(T, \mathbf{R}) = \mathrm{Tr}\{U_t[t \to t + T; \mathbf{r}]^\dagger U_s[t; \mathbf{r} \to \mathbf{r} + \mathbf{R}] \times U_t[t \to t + T; \mathbf{r} + \mathbf{R}] \times U_s[t + T; \mathbf{r} \to \mathbf{r} + \mathbf{R}]^\dagger\}. \quad (58)$$

The off-axis component $U_s[t; \mathbf{r} \to \mathbf{r} + \mathbf{R}]$ is computed following the algorithm in Ref. [81]. In order to reduce the noise in the static potential, we build the Wilson loops with smeared link variables. We choose a single step of hypercubic (HYP) smearing [82]; the smeared link variable is a function of all the links belonging to the unit hypercubes adjacent to the original link. We found the HYP smearing effective enough for our purposes, even not implementing a variational method. The main disadvantage is that it deforms the static potential at short distances; however it does not affect the determination of the string tension, which is our main goal.

In the Hamiltonian gauge $[U(x, 0) = 1]$, the expectation value of $W(T, \mathbf{R})$ becomes the time correlator for the

operator $M(\mathbf{R}) = \bar{Q}(\mathbf{r})U_s[\mathbf{r} \to \mathbf{r} + \mathbf{R}]Q(\mathbf{r} + \mathbf{R})$ which creates a heavy quark-antiquark pair connected by a string:

$$\langle W(T, \mathbf{R})\rangle = \frac{1}{Z(L_t)} \mathrm{Tr}[e^{-(L_t-T)H} M(\mathbf{R})^\dagger e^{-TH} M(\mathbf{R})] = \frac{1}{Z(L_t)} \sum_{nm} |\langle n, \mathbf{R}|M(\mathbf{R})|m\rangle|^2 \times e^{-L_t E_m} e^{-T[V_n(R)-E_m]}, \quad (59)$$

where we have inserted the gauge-invariant states $|m\rangle$ with energy E_m, and the states in the presence of a quark-antiquark pair $|n, \mathbf{R}\rangle$ with energy $V_n(R)$. The energy $V_0(R)$ of the fundamental state in the presence of the quark-antiquark pair is the static potential. $Z(L_t)$ is the partition function, which can be decomposed in terms of the gauge-invariant states $|m\rangle$:

$$Z(L_t) = \mathrm{Tr} e^{-L_t H} = \sum_m e^{-L_t E_m}. \quad (60)$$

If the temporal extension L_t is large enough, we can identify three regimes for the Wilson loops while T changes:

(1) Small values of T with respect to the temporal extension ($T \ll L_t$). This is the usual zero temperature limit. In this case only the vacuum survives among the $|m\rangle$ states:

$$\langle W(T, \mathbf{R})\rangle \simeq \sum_n |\alpha_n(R)|^2 e^{-T[V_n(R)-E_0]}, \quad \text{with} \quad \sum_n |\alpha_n(R)|^2 = 2, \quad (61)$$

where the relationship for the coefficients α_n comes from $\langle W(0, \mathbf{R})\rangle = 2$. It is interesting to notice that, since $\langle W(T, \mathbf{R})\rangle \leq 2$ for each value of T, $V_n(R)$ must be larger than the vacuum energy E_0 for each value of $R > 0$ (because of the lattice discretization, the potential is bounded from below). Therefore in this regime, the Wilson loop is decreasing in T at every fixed $\mathbf{R}$.

(2) Values of T comparable with the temporal extension ($L_t - T \ll L_t$). In this case only the $|0, \mathbf{R}\rangle$ survives among the states with external charges:

$$\langle W(T, \mathbf{R})\rangle \simeq e^{-L_t[V_0(R)-E_0]} \sum_m |\beta_m(R)|^2 \times e^{-(L_t-T)[E_m-V_0(R)]}. \quad (62)$$

Assume that the sum is dominated by some m. If the quantity $E_m - V_0(R)$ is positive, the Wilson loop at fixed $\mathbf{R}$ is increasing as T approaches L_t, toward its extremal value $\langle W(L_t, \mathbf{R})\rangle \simeq \sum_m |\beta_m(R)|^2 \leq 2$. If the quantity $E_m - V_0(R)$ is negative, the Wilson loop at fixed $\mathbf{R}$ is decreasing toward its extremal value. Notice that, since the states propagating around the torus are not the same as the ones propagating inside the Wilson loop, the Wilson loop is not symmetric in T around $L_t/2$ as usually happens for other correlators.

(3) Intermediate values of T ($a \ll T \ll L_t$). In this case the Wilson loop reduces to a single exponential:

$$\langle W(T, \mathbf{R})\rangle \simeq A(\mathbf{R}) e^{-T[V_0(R)-E_0]}. \quad (63)$$

This is the useful regime which we will try to identify in our numerical simulations to extract the static potential.

The first and second regions are always visible if the temporal length T of the Wilson loop is too small or too large. With the extra difficulty that the Wilson loops are not symmetric in $T \to L_t - T$, the computational problem for the static potential is similar to the one for other correlators: it is important to have a large enough lattice in such a way that the third region opens up in the middle. An effective potential is therefore defined, with the property that it shows a plateau in the third region (if visible), and the value of the plateau is actually the static potential. We use two different methods to extract the effective potential from the Wilson loops.

(i) *Potential 1:* The easiest method consists of defining an effective potential as

$$V_{\mathrm{eff}}(T, \mathbf{R}) = -\frac{1}{a} \log \frac{\langle W(T + a, \mathbf{R})\rangle}{\langle W(T, \mathbf{R})\rangle}. \quad (64)$$

If we can see a plateau in the effective potential as a function of T, it means that we can isolate the single-exponential region. The value $V(\mathbf{R})$ is then extracted by fitting the plateau of the effective potential with a constant. Notice that since the lattice breaks rotational invariance, we consider the potential as a function of $\mathbf{R}$, and not of its module only. An unbiased estimate for the average of the potential and an estimate of its error are obtained by applying Eq. (64) to a set of bootstrap ensembles.

(ii) *Potential 2:* When the single-exponential region is not visible, we use the Prony's method [83] for taking into account also the first excited state. We refer to the literature for the general idea, while we summarize here the used formulas. Having chosen a value of $\mathbf{R}$, for every value of T we solve the following second-order equation:

$$[W(T, \mathbf{R})W(T + 2a, \mathbf{R}) - W(T + a, \mathbf{R})^2]x^2 \quad (65)$$

$$+ [W(T + a, \mathbf{R})W(T + 2a, \mathbf{R}) - W(T, \mathbf{R})W(T + 3a, \mathbf{R})]x \quad (66)$$

$$+ [W(T + a, \mathbf{R})W(T + 3a, \mathbf{R}) - W(T + 2a, \mathbf{R})^2] = 0. \quad (67)$$

If x_0 is the largest solution (but smaller than 1), we define an effective potential as

$$V_{\rm eff}(T, \mathbf{R}) = -\frac{1}{a}\log x_0. \tag{68}$$

As for the previous method, the value $V(\mathbf{R})$ is extracted by fitting the plateau of the effective potential with a constant. The whole procedure is implemented via a bootstrap, in order to get an unbiased estimate for the average of the energies, and an estimate of its error.

Whenever we can compute the potential with both methods we observe that they always give compatible results, but slightly smaller errors and better determinations of the plateaus are obtained with the method Potential 2. Even though the string tension can be in principle extracted from a linear fit of the static potential in a large-distance region, it is instructive to determine it also from the force $F = -\frac{dV}{dR}$. At large R, $F \sim \sigma$. For the determination of F, we use the following methods.

(i) *Force 1:* We use generalized Creutz ratios to define an effective force with off-axis Wilson loops:

$$F_{\rm eff}(T, \mathbf{R}, a\mathbf{n}) = -\frac{1}{a^2|\mathbf{n}|}\log\frac{\langle W(T+a, \mathbf{R}+a\mathbf{n})\rangle\langle W(T, \mathbf{R})\rangle}{\langle W(T, \mathbf{R}+a\mathbf{n})\rangle\langle W(T+a, \mathbf{R})\rangle}. \tag{69}$$

We use $\mathbf{n}$ vectors of the form (1,0,0), (1,1,0), and (1,1,1) and permutations. We identify the plateau of the effective force as a function of T, and we fit it with a constant $F(R_I)$. The statistical error is determined by a bootstrap procedure. The improved distance R_I is defined as in Ref. [84] to be

$$R_I = \left| 4\pi \frac{G(\mathbf{R}+\mathbf{n}) - G(\mathbf{R})}{a|\mathbf{n}|} \right|^{-1/2}, \tag{70}$$

where $G(\mathbf{R})$ is the three-dimensional free-scalar propagator on the lattice.

(ii) *Force 2:* Plateaus in the Creutz ratios are visible only in a region where only a single exponent dominates in the expansion of the Wilson loop. In most of the cases we need to take into account the first excited state. An effective force can be defined by using the effective potentials computed by the method Potential 2:

$$F_{\rm eff}(T, \mathbf{R}, a\mathbf{n}) = -\frac{V_{\rm eff}(T, \mathbf{R}+a\mathbf{n}) - V_{\rm eff}(T, \mathbf{R})}{a|\mathbf{n}|}. \tag{71}$$

We identify the plateau of the effective force as a function of T, and we fit it with a constant $F(R_I)$. Expectation value and error of $F(R_I)$ are estimated by means of a bootstrap procedure.

The static potentials presented in this section have been computed with the method Potential 2. In Fig. 6, two typical effective potentials are shown, together with the fit range and the result of the constant fit.

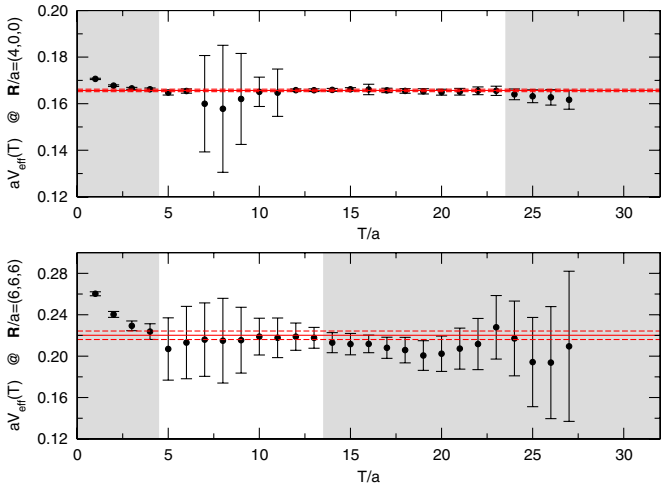

FIG. 6 (color online). Effective potentials at $\mathbf{R} = (4a, 0, 0)$ and $\mathbf{R} = (6a, 6a, 6a)$ computed on the 32×16^3 lattice at bare mass $am_0 = -1.15$. Plateaus have been chosen in the white regions. The red lines represent the values of the potential (with errors), obtained by fitting the effective potential with a constant in the white region. Errors have been computed with a bootstrap procedure.

The static potentials for all the simulations listed in the last column of Table IV are plotted in Fig. 7. The corresponding forces are separately plotted in Fig. 8. Although in principle the static potential or the force can be used to extract the string tension, in practice a reliable result cannot be obtained from those quantities, the most likely

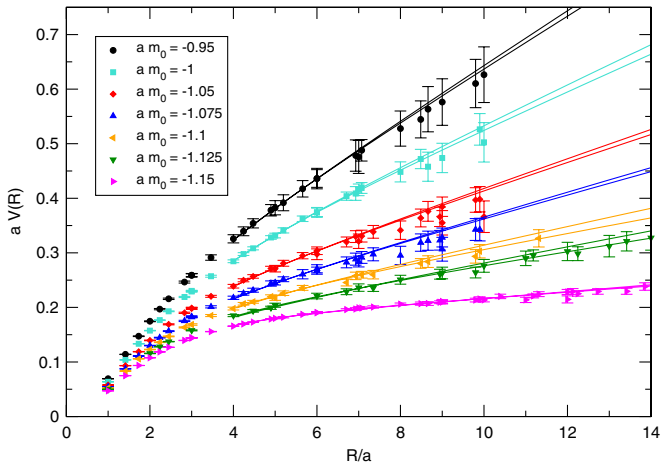

FIG. 7 (color online). Static potentials computed with the method Potential 2 (see Sec. VI) from Wilson loops with HYP smearing. Data for bare masses -0.95, -1, -1.05, -1.075, and -1.1 are obtained on a 24×12^3 lattice; data for bare mass -1.125 are obtained on a $24 \times 24 \times 12^2$ lattice; data for bare mass -1.15 are obtained on a 32×16^3 lattice. Superimposed is the function $V(R) = \sigma R + \mu + c/R$, where σ has been taken from Table IV (the two curves correspond to $\sigma - \Delta\sigma$ and $\sigma + \Delta\sigma$), while μ and c have been obtained with a fit in the region $R \geq 3a$.

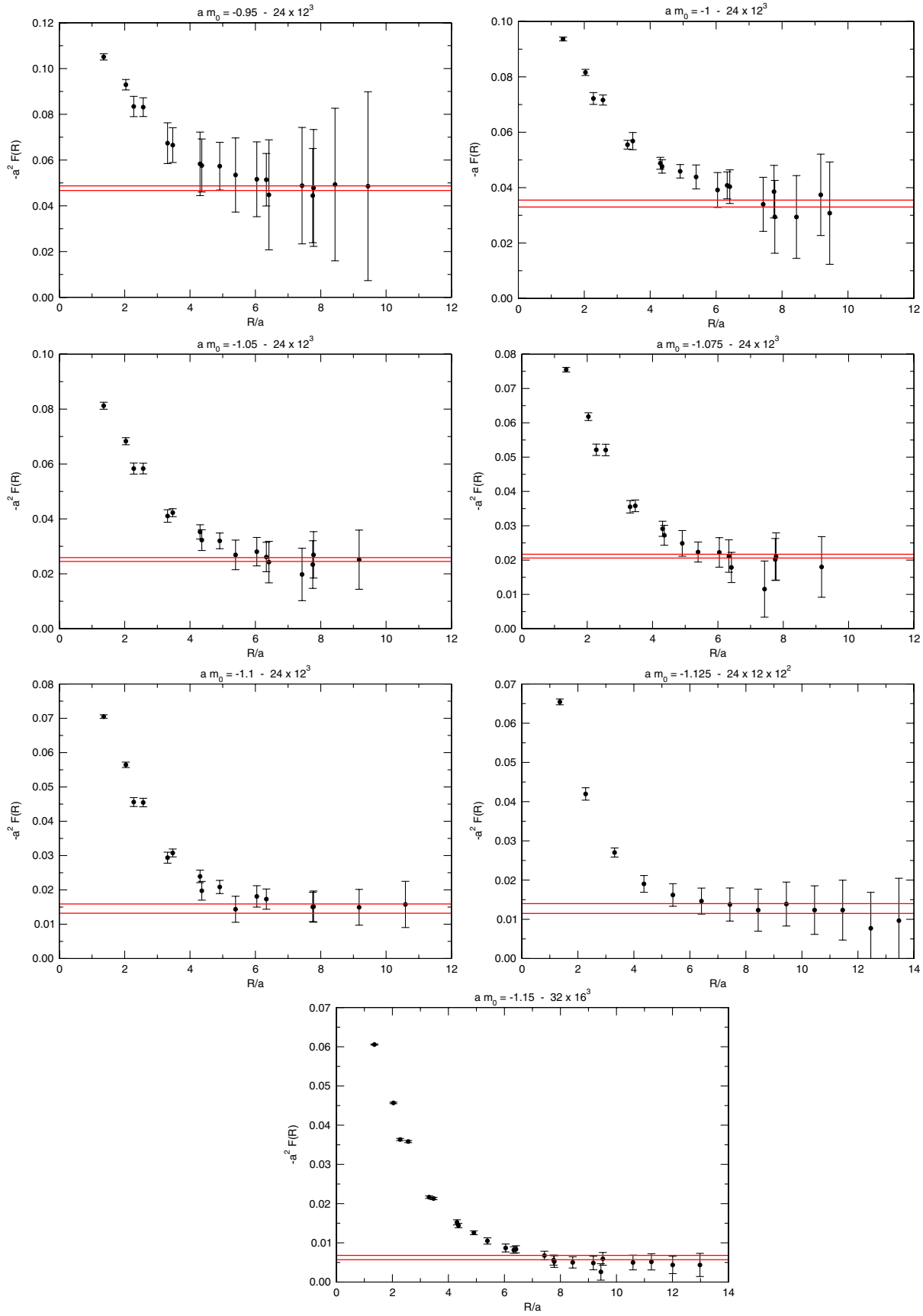

FIG. 8 (color online). Forces computed with the method Force 2 (see Sec. VI). Superimposed is the string tension from Table IV.

explanation being either that our data are not accurate enough or that the lattice sizes explored are too small for the plateau to be free from systematic errors. A variational procedure like the one used for extracting the string tension from correlators of Polyakov loops (described in Sec. V) might be helpful also for the static potential computation. Although we are unable to perform a comparison between the string tensions extracted with the two different methods, we can still check that the static potentials and the forces are compatible with the string tensions reported in Table IV.

We fit the static potential with the function:

$$V(R) = \sigma R + \mu + \frac{c}{R}, \tag{72}$$

assuming the string tensions shown in Table IV, in the range $R \geq 3a$. The results of the fits are shown in Fig. 7. Since we do not want to assume at this stage a particular effective string theory (and anyhow the HYP smearing introduces spurious $1/R$ effects), the coefficient of the $1/R$ term becomes an extra parameter in the fitting procedure. In all the cases we have investigated, the string tension computed via Polyakov loop correlators captures correctly the large-distance behavior of the static potential.

In Fig. 8, the forces are plotted together with the values of the string tension. Although the errors on the force are in some cases quite large and only qualitative statements are possible, it can be seen also in this case that the string tension computed via Polyakov loop correlators always captures the large-distance behavior of the force itself. The force always shows plateaus at large distances, with a central value often in striking agreement with the string tension computed from Polyakov loop correlators. This might indicate that our analysis overestimates the statistical errors.

VII. GLUEBALLS

Glueball masses are extracted from a variational procedure similar to the one used for Polyakov loops and based on the same fuzzying scheme. At the link level, we consider a collection of closed elementary loops transforming according to the irreducible representations of the symmetry group of the cube, to which rotational symmetry is broken on the lattice [85]. The variational procedure is then built by replacing the original links with those obtained after smearing and blocking. Then, in each channel a matrix of connected correlators is constructed, whose eigenvectors with the highest eigenvalues are almost the pure eigenstates of the Hamiltonian with the lowest masses. We have implemented this technique using as starting operators the plaquette and the length-six planar closed contour to build the A, E, and T irreducible representations of the cubic group. The lowest-lying state in the A channel corresponds to the lightest 0^{++} glueball in the continuum limit, while both the E and the T lightest states give the lightest 2^{++} glueball mass in the continuum limit.

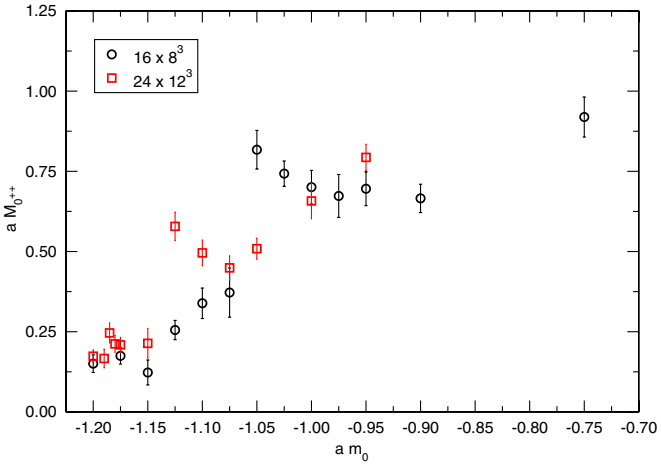

FIG. 9 (color online). The mass of the 0^{++} glueball in lattice units, $aM_{0^{++}}$, measured at various values of bare quark mass am_0 on a 16×8^3 and on a 24×12^3 lattice.

Our results for the 0^{++} glueball are illustrated in Fig. 9. We discuss only the results on the 16×8^3 and the 24×12^3 lattices, since on the 32×16^3 lattice for all values of the simulated bare fermion masses our system is in the A phase. As it can be seen from the plot, as am_0 is decreased, in the S phase $aM_{0^{++}}$ monotonically decreases. When the system starts to develop double peaks for the Polyakov loop distribution in a spatial direction, the mass of the 0^{++} glueball first goes to a short plateau and then moderately increases, to drop dramatically to much lower values at lower am_0. The overlap between the masses measured on the two lattices at $am_0 = -0.95$ suggests that as long as we stay in the symmetric phase, finite-size effects are under control. Hence, as our best estimate for the infinite-volume limit of $aM_{0^{++}}$, we take the values on the 16×8^3 lattice for $am_0 > -0.95$ and the values on the 24×12^3 lattice for $-1.05 \leq am_0 \leq -0.95$. Since for $am_0 < -1.05$ in both cases our system is in the A phase,

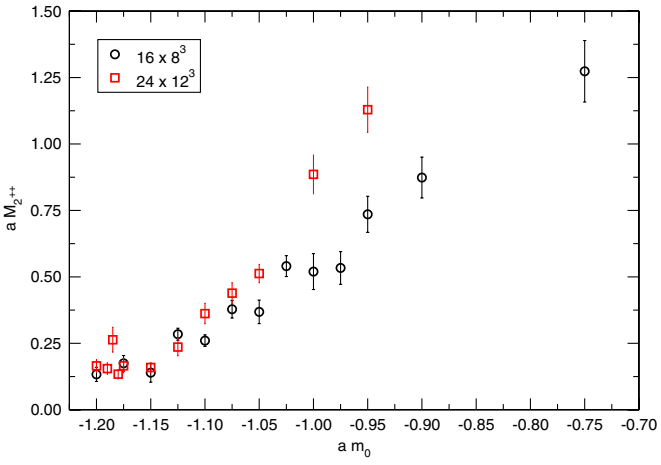

FIG. 10 (color online). The mass of the 2^{++} glueball in lattice units, $aM_{2^{++}}$, measured at various values of bare quark mass am_0 on a 16×8^3 and on a 24×12^3 lattice.

TABLE V. Infinite-volume estimates of $aM_{0^{++}}$ and $aM_{2^{++}}$. Values extracted on a 16×8^3 lattice have been used for $am_0 > -0.95$ and values extracted on a 24×12^3 lattice for $am_0 \leq -0.95$.

$-am_0$	$aM_{0^{++}}$	$aM_{2^{++}}$
−0.25	1.159(98)	2.18(22)
0.25	1.108(97)	1.92(22)
0.5	1.045(70)	1.93(19)
0.75	0.919(63)	1.27(12)
0.9	0.666(44)	0.874(77)
0.95	0.793(41)	1.129(85)
1	0.658(56)	0.886(73)
1.05	0.510(33)	0.513(35)

we do not take into account the corresponding values of $am_{0^{++}}$ in the following analysis.

The mass of the 2^{++} glueball as a function of am_0 is shown in Fig. 10. These results have been obtained using operators transforming according to the E representation of the cubic group. Our analysis in the T channel gives compatible results in all cases. Our data show that the 2^{++} glueball is heavier than the 0^{++} in the symmetric phase, but dramatically decreases to very low values of the mass (well below the mass of the 0^{++}) at the onset of the A phase. Deeper in the A phase, the two states appear to be degenerate. As the figure shows, no good control over finite-size effects can be reached on our lattices for the 2^{++} mass. For the sake of completeness, we still provide an estimate for its mass at infinite volume, but this is likely to be quite rough. Hence, the 2^{++} glueball will play a marginal role in the interpretation of our results.

Our numerical estimates of $aM_{0^{++}}$ and $aM_{2^{++}}$ in the infinite-volume limit are reported in Table V. The degeneracy between the two states at $m = -1.05$ together with the impossibility of establishing whether the system is in the S phase (see Table II) would suggest to disregard glueball masses at this value of the bare mass. However, since this point was part of our analysis in Ref. [57], where the lower statistics masked the issue, in order to facilitate a comparison with our previous work, we chose to keep it also in our current analysis. The reader should bear this in mind for the discussion of our results.

VIII. HYPERSCALING SCENARIO AND LOCKING SCALE

Our infinite-volume estimates for the PS (at each value of the bare mass, we choose the PS mass computed on the largest volume in [58]), the 0^{++} and the 2^{++} glueball masses, and $\sigma^{1/2}$ as a function of the partially conserved axial current (PCAC) mass am (see Refs. [19,58] for a definition of this quantity) are reported in Fig. 11. As noticed in Ref. [57], the data show a clear hierarchy in the spectrum, with the mesonic scale well above the gluonic scale. Since over the range of investigated masses $a\sigma^{1/2}$ changes by a factor of 5, the effect of the fermion

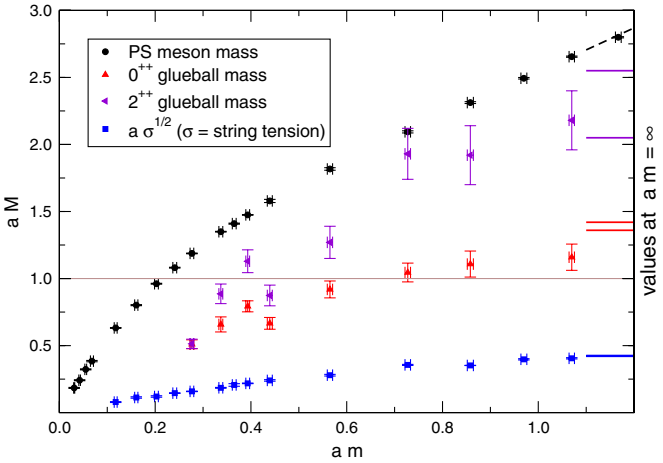

FIG. 11 (color online). The spectrum of the theory as a function of the PCAC mass am. The mass of the vector is not shown, since on the scale of the figure this state appears to be degenerate with the PS.

determinant as the mass is decreased is an essential component of the dynamics in this theory. Hence, the simple quenched scenario, according to which the theory would be QCD like and the hierarchy in the spectrum is due to large fermion masses, can be excluded. In fact, the spectrum looks similar to the hyperscaling scenario at high locking mass $M_{\rm lock}$ sketched in Fig. 1 (right panel). In this section we shall show that indeed that scenario provides the right description of the spectrum of this theory.

Up to subleading corrections, the hyperscaling scenario implies the independence of ratios of physical quantities from the fermion mass in the scaling region. In Fig. 12 we plot the ratio $M_{\rm PS}/\sigma^{1/2}$. This quantity shows a plateau $M_{\rm PS}/\sigma^{1/2} \simeq 7.5$ for $aM_{\rm PS} \leq 1.25$, supporting the idea that gluonic and fermionic masses are not parametrically independent in this region but are both proportional to the RG-invariant fermion mass M (again, this is what we are calling locking). The independence from M of the ratio of

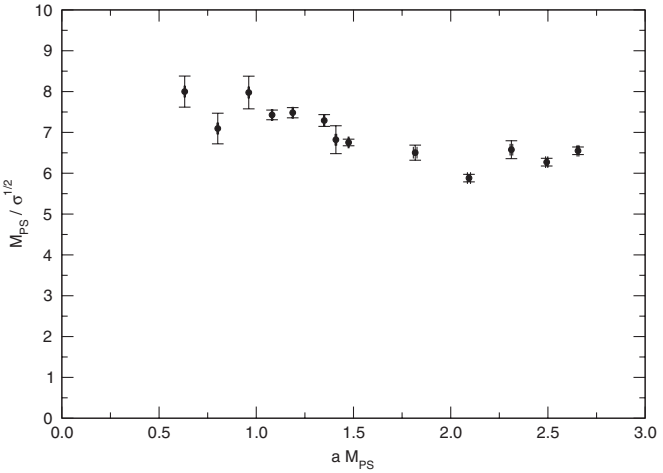

FIG. 12. The ratio $M_{\rm PS}/\sigma^{1/2}$ as a function of $M_{\rm PS}$.

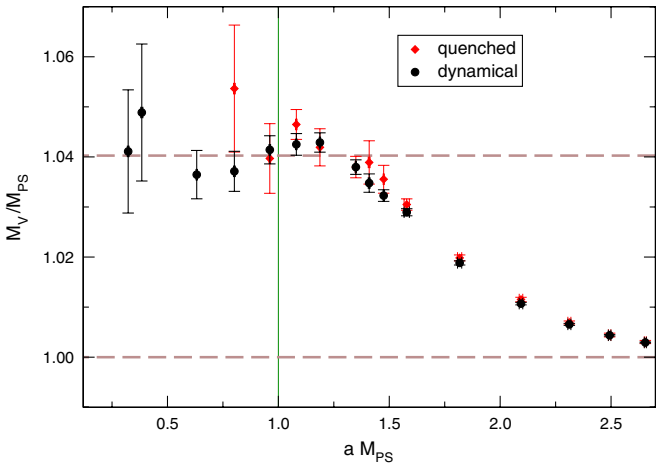

FIG. 13 (color online). Comparison of the ratio M_V/M_{PS} as a function of aM_{PS} in the quenched and the dynamical theory. The dynamical ratio approaches the infinite-mass value of 1 at large aM_{PS} and develops a plateau (signaling hyperscaling) at $aM_{PS} \leq 1.25$.

spectral quantities in the scaling region can be observed also in the ratio M_V/M_{PS} (Fig. 13). Again a plateau develops for $aM_{PS} \leq 1.25$. The existence of these plateaus is a clear indication of the spectrum behaving as predicted by hyperscaling. Moreover, the value of both $M_{PS}/\sigma^{1/2}$ and M_V/M_{PS} in the scaling region suggests that the locking scale M_{lock} is large. If this is the case, $SU(2)$ gauge theory with two adjoint Dirac fermions should look like a heavy fermion system for all values of the fermion mass.

In order to verify this scenario, we can compare our dynamical results with results obtained in the quenched theory. In this process, a crucial point is to match properly the bare parameters in the two theories, since the physics of the dynamical and quenched systems is expected to be equivalent once the physical scale is matched [see Eq. (32)]. For this reason, we need to tune the bare parameters of the quenched simulations, namely, the gauge coupling $\beta^{(q)}$, and the mass of the valence fermion $am_0^{(q)}$, so that we can match two independent quantities between the two theories. For this matching, it is convenient to choose two observables with a sharp dependency on each of the bare parameters, in order to achieve the best possible tuning between the two theories. In our study, we have required the quantities $a\sigma^{1/2}$ and aM_{PS} to be equal in the dynamical and in the quenched systems. Given that in the dynamical theory with adjoint fermions the fundamental string cannot break, this quantity is a natural candidate to fix the coupling $\beta^{(q)}$ in the quenched simulation. As far as the valence quark mass $am_0^{(q)}$ is concerned, we chose to determine the quenched value by fixing the pseudoscalar mass, because in the fermionic sector this is the quantity we have the best control over.

The procedure to compare the quenched and dynamical theories requires the following steps:

(1) find the value $\beta^{(q)}$ of the coupling for the quenched theory, in such a way that the string tension in lattice units matches the dynamical value;
(2) find the value $am_0^{(q)}$ of the bare fermion mass for the quenched theory, in such a way that the PS meson mass matches the dynamical value aM_{PS};
(3) compute the rest of the spectrum, for example, the ratio of the PS and V meson masses or the glueball masses, in the dynamical theory with bare parameters (β, am_0) and in the quenched theory with bare parameters $(\beta^{(q)}, am_0^{(q)})$, and compare the results.

In practice the program as outlined above requires a fine-tuning of the bare parameters, and turns out to be a highly expensive computational task. Instead of an exact matching of the parameters, we have performed a scan in the parameters of the quenched theory. The lattice parameters at which quenched simulations have been performed are reported in Table VI. The range of the scan of $\beta^{(q)}$ is chosen in order to include all the string tension values of our dynamical simulations. The upper bound of this window is simply given by $\beta \equiv 2.25$, the value of β for our dynamical simulations. This is a consequence of the string

TABLE VI. Bare parameters and volumes used for quenched simulations. For each $\beta^{(q)}$ we report also the measured string tension.

$\beta^{(q)}$	$a\sigma^{1/2}$	V	$am_0^{(q)}$
2.25	0.423 1(25)	24×12^3	$-1.65, -1.6, -1.55, -1.5, -1.45, -1.4, -1.35, -1.3, -1.25, -1.2, -1.175, -1.15, -1.125, -1.1, -1.075, -1.05, -1.025, -1.0, -0.75, -0.5, -0.25, 0.0, 0.25, 0.5$
2.4265	0.238 8(9)	24×12^3	$-1.2, -1.175, -1.15, -1.125, -1.1, -1.075, -1.05, -1.025, -1.0, -0.75, -0.5, -0.25, 0.0, 0.25, 0.5$
2.5115	0.176 8(8)	24×12^3	$-1.2, -1.175, -1.15, -1.125, -1.1, -1.075, -1.05, -1.025, -1.0, -0.75, -0.5, -0.25, 0.0, 0.25, 0.5$
2.6	0.133 95(62)	24×12^3	$-1.2, -1.175, -1.15, -1.125, -1.1, -1.075, -1.05, -1.025, -1.0, -0.75, -0.5, -0.25, 0.0, 0.25, 0.5$
2.62	0.125 8(7)	24×12^3	$-1.3, -1.25, -1.2, -1.15, -1.1, -1.05, -1.0, -0.75, -0.5, -0.25, 0.0, 0.25, 0.5$
2.68	0.103 5(7)	32×32^3	$-1.25, -1.2, -1.15, -1.1, -1.05, -1, -0.95, -0.9, -0.85, -0.8, -0.75, -0.5$

tension being an increasing function of the bare fermion mass, so an infinite-mass simulation corresponds to a string tension of a pure gauge system at the same $\beta \equiv 2.25$.

For each choice of $\beta^{(q)}$ we measure the string tension and the 0^{++} and 2^{++} glueball masses (following e.g. Ref. [74]). Quenched glueball masses have been interpolated using the ansatz

$$\frac{M_{\mathrm{G}}}{\sigma^{1/2}} = A_0 + A_1 a^2 \sigma, \tag{73}$$

with A_0 and A_1, respectively, the leading (constant) and subleading [$\mathcal{O}(a^2)$] coefficients in the extrapolation to the continuum limit.

On the same gauge configurations, we measure the quenched PS mass and the $M_{\mathrm{V}}/M_{\mathrm{PS}}$ ratio, for a set of values of $am_0^{(q)}$ covering the entire interval of PS masses appearing in the dynamical calculation. We then create an interpolating function for the central value of the ratio $M_{\mathrm{V}}/M_{\mathrm{PS}}$.

To obtain an error on this estimate, we create two other interpolating functions for the maximal and the minimal value of the quenched estimate $M_{\mathrm{V}}/M_{\mathrm{PS}}$ set by the statistical error, so that for each choice of the pair $(M_{\mathrm{PS}}, \sigma)$, we can read the corresponding range of values for $M_{\mathrm{V}}/M_{\mathrm{PS}}$. To take into account the indetermination in our estimate of aM_{PS} and $a^2\sigma$, we consider a region within 1σ around the central value for those quantities: in this region the difference between the maximum value of the maximal interpolating function and the minimum of the minimal interpolating function provides us with an estimate for the error on $M_{\mathrm{V}}/M_{\mathrm{PS}}$ in the quenched theory.

By means of the interpolating functions, we can read the value of $M_{\mathrm{G}}/\sqrt{\sigma}$ and $M_{\mathrm{V}}/M_{\mathrm{PS}}$ in the quenched simulations at values of $a\sqrt{\sigma}$ and aM_{PS} (the latter being relevant only for the $M_{\mathrm{V}}/M_{\mathrm{PS}}$ ratio) obtained in the dynamical simulations.

In Table VII we report the values of the mass of the glueballs for the quenched theory at the values of the string tension obtained in the dynamical theory. In Fig. 14 we show the comparison between the dynamical glueball values and the interpolating functions obtained from the quenched theory. Except for the last point, for which, as discussed in Sec. VII, the dynamical simulations are probably in the A phase, the agreement between the quenched and dynamical spectra at the same physical scale (in units of the ultraviolet cutoff) is striking. This supports the idea that the low-energy dynamics of the theory with dynamical fermions is well described by a pure Yang-Mills theory,

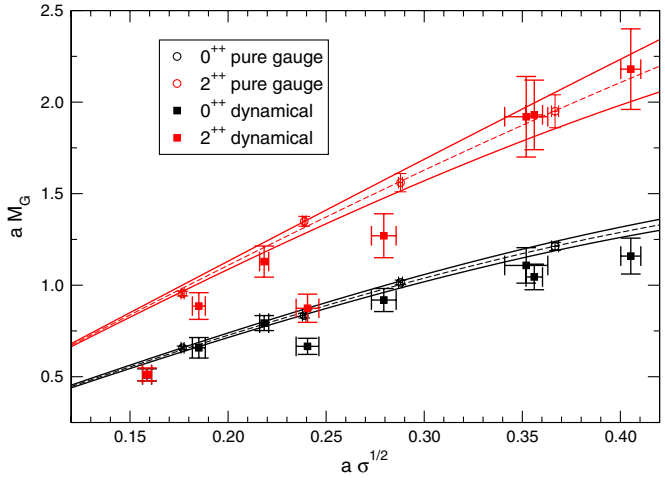

FIG. 14 (color online). Comparison of the masses of glueballs of the dynamical theory with the interpolating functions of the quenched theory. Among the plotted data, the dynamical points at $a\sigma^{1/2} = 0.2405(58)$ and $a\sigma^{1/2} = 0.1587(23)$ correspond to the lightest masses, respectively, on the 16×8^3 and 24×12^3 lattices. Hence, the glueball masses for those string tensions are affected by the largest finite-size effects.

TABLE VII. The results of the interpolation procedure for the quenched data of the mass of the glueballs at the values of $a\sigma^{1/2}$ equal to the ones found in the dynamical simulations. The errors in the third column have been obtained from the variation of the numerical results on the maximal and the minimal interpolating functions.

$a\sigma^{1/2}$	$aM_{0^{++}}^{(q)}$	$aM_{2^{++}}^{(q)}$
0.4053(51)	1.30(4)	2.13(15)
0.352(11)	1.18(5)	1.89(14)
0.3561(42)	1.185(35)	1.90(11)
0.2794(63)	0.975(35)	1.53(8)
0.2405(58)	0.855(35)	1.325(65)
0.2184(23)	0.785(15)	1.21(4)
0.1851(33)	0.675(25)	1.025(35)
0.1587(23)	0.585(15)	0.885(25)

TABLE VIII. The results of the interpolation procedure for the quenched data of $M_{\mathrm{V}}^{(q)}/M_{\mathrm{PS}}^{(q)}$ at the values of $a\sigma^{1/2}$ and aM_{PS} equal to the ones found in the dynamical simulations. The errors in the third column have been obtained from the variation of the numerical results on the maximal and the minimal interpolating functions.

$a\sigma^{1/2}$	aM_{PS}	$M_{\mathrm{V}}^{(q)}/M_{\mathrm{PS}}^{(q)}$
0.4053(51)	2.6546(47)	1.003 03(32)
0.3976(51)	2.4936(57)	1.004 42(38)
0.352(11)	2.3120(68)	1.006 93(30)
0.3561(42)	2.0939(80)	1.011 52(44)
0.2794(63)	1.8172(95)	1.019 83(59)
0.2405(58)	1.579(12)	1.030 4(11)
0.2184(23)	1.4748(24)	1.035 5(27)
0.2066(97)	1.4094(42)	1.038 9(40)
0.1851(33)	1.3493(28)	1.037 9(21)
0.1587(23)	1.1874(28)	1.041 9(37)
0.1455(19)	1.0811(31)	1.046 4(30)
0.1205(56)	0.9613(35)	1.039 6(70)
0.1130(54)	0.8017(41)	1.053(13)

which is evidence for a locking mechanism with a large $M_{\rm lock}$ taking place in this theory.

The relevant interpolated quenched results for the ratio $M_{\rm V}/M_{\rm PS}$ as a function of $M_{\rm PS}$ are reported in Table VIII and compared with the dynamical results in Fig. 13. The quenched and dynamical data have a remarkable overlap for all the points except for the last one, where strong finite-size effects are expected to affect both the quenched and the dynamical simulations. Together with the plateau in the ratio developing for $aM_{\rm PS} \leq 1.25$, the comparison confirms once again a locking mechanism taking place at large $M_{\rm lock}$.

IX. THE CHIRAL CONDENSATE ANOMALOUS DIMENSION

The hyperscaling scenario supported by our data seems to imply the existence of an infrared fixed point. However, since the evidence for the hyperscaling and the locking of the mesonic and gluonic spectra is still over a small range of am, simulations at smaller masses and large volumes are needed to confirm the trend identified so far.

If the theory is IR conformal, all the spectral quantities scale as m^ρ for a unique value of $\rho = 1/(1+\gamma_*)$, with γ_* the anomalous dimension of the condensate. Hence, in this case γ_* is physically well defined.

In order to build phenomenologically viable technicolor models, a large anomalous dimension is generally required. From a purely theoretical point of view $0 \leq \gamma_* \leq 2$, where $\gamma_* = 0$ corresponds to the noninteracting case and $\gamma_* = 2$ is the bound imposed by unitarity; a value $\gamma_* \approx 1$ might reconcile technicolor with high-precision data for the standard model. The determination of γ_* is then one of the goals of lattice simulations of BSM strong dynamics.

In order for us to be able to extract a scaling exponent, the simulations must be performed in a region of sufficiently small masses. The exact extent of the scaling region (which also depends on the observable being analyzed) is only known *a posteriori*. On the lattice, the problem is complicated by the explicit breaking of conformal invariance due to the finite size of the system. This can however be turned into a powerful tool for determining the exponent of the scaling with the mass using a technique commonly known in statistical bechanics as *finite-size scaling* (FSS). FSS states that the dimension of the system is a relevant scaling variable with mass dimension -1. Hence, the asymptotic scaling formula

$$aM_X \propto (am)^\rho, \qquad \rho = 1/(1+\gamma_*), \tag{74}$$

where M_X is a spectral quantity of the system, on a finite lattice of spatial extension $L_s = aN_s$ and in the regime $L_s \to \infty$ and $m \to 0$ becomes

$$M_X L_s = f(x), \qquad x = N_s(am)^\rho, \tag{75}$$

i.e. the product $M_X L_s$ is a universal function of the scaling variable x. A simple consequence is that the ratio of two spectral quantities is expected to be a universal function of $M_X L_s$ for any spectral quantity M_X. Note that this is true for both the S and the A phases of the system. In Fig. 15 we show the ratio $\sigma_t^{1/2}/M_{\rm PS}$ as a function of $M_{\rm PS}L_s$. The universality of the ratio is verified up to values of $M_{\rm PS}L_s \simeq 12$.

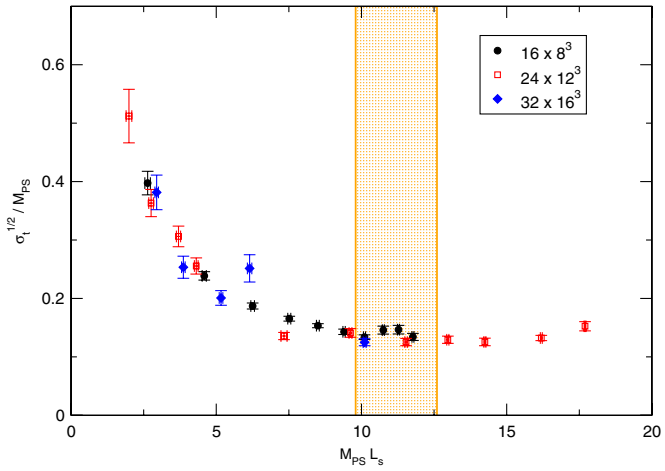

FIG. 15 (color online). The ratio $\sigma_t^{1/2}/M_{\rm PS}$ as a function of $M_{\rm PS}L_s$ at various lattice sizes. In the shaded region the crossover between the S and the A phase takes place.

If the system is in the scaling region (for which we have support from our data) and the infinite-volume estimates for spectral quantities are correct, Eq. (74) can be used for determining γ_*. We have shown in Sec. V that our determination of the string tension is reasonably under control. Hence, we perform a fit of our data for $\sigma^{1/2}$ using Eq. (74). With a good quality of the fit (see Fig. 16), we find $\gamma_* = 0.22(6)$. Both horizontal and vertical data errors have been taken into account by implementing a bootstrap procedure. The fit has been performed on the lightest four points, and

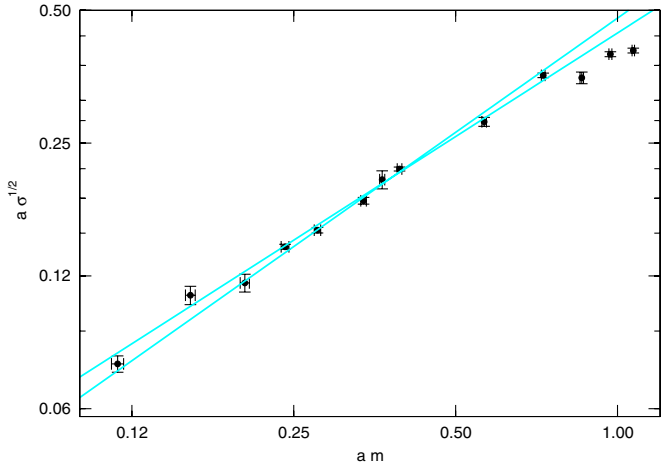

FIG. 16 (color online). $a\sigma^{1/2}$ as a function of am. A fit of the data to Eq. (74) is also shown. In particular, the two lines represent the extremal values $\gamma_* = 0.16$ and $\gamma_* = 0.28$.

then progressively increasing the fitting region to include ten points (all but the last three in Fig. 16). No systematic trend has been observed when enlarging the fitting region. The quoted value of γ_* is a conservative estimate compatible with all the values obtained using the fitting procedure described above.

The value we find for γ_* is compatible with determinations obtained in the same theory using other quantities (e.g. related to mesonic physics [58]) or independent techniques like the Schröedinger functional [29]. These results clearly favor the existence of a genuine IR fixed point for this theory. The fact that independent measurements of γ_* fall all in the same window of values is a clear message for model building.

X. CONCLUSIONS

In this work, using numerical simulations of the lattice model for several sizes of the system and a wide range of fermion masses, we have shown that at sufficiently low masses the spectrum of minimal Wwalking technicolor is consistent with the existence of an infrared fixed point. In particular, for this specific realization of locking, the theory at large distances is isospectral to a Yang-Mills $SU(2)$ theory, where the dynamically generated scale of the pure gauge theory is determined by the fermion mass in minimal walking technicolor, and turns out to be smaller than the latter. To confirm this scenario would require one to extend our study to much smaller fermion masses, down to values that are not accessible at present to lattice simulations. Another technical limitation of our study is the simulation at a fixed value of β: in order to verify that lattice artifacts are not distorting the physical picture, further studies closer to the continuum limit should be performed.

Assuming the existence of the IR fixed point, we have determined the anomalous dimension of the condensate, which is found to be $\gamma_* = 0.22(6)$. This value is in agreement with other independent determinations, which strengthen the conclusions that the theory is infrared conformal. The value of γ_* for this theory is probably too small for conventional technicolor scenarios, although alternative scenarios compatible with a small anomalous dimension can be devised (see e.g. [86]). It would be desirable to include larger lattices in our FSS analysis.

Finally, we notice that a FSS analysis performed in a $SU(3)$ gauge theory with two fermion flavors in the two-index symmetric representation [which for $SU(2)$ coincides with the adjoint representation] finds $\gamma_* \simeq 0.5$ [31]. Assuming that, as stated in Refs. [24,25], this theory is infrared conformal (however, see Refs. [35,36] for alternative scenarios), this might imply that γ_* for two-index symmetric fermions is an increasing function of the number of colors N. If this is the case, it would be interesting to determine whether γ_* becomes of order 1 for large enough values of N and whether γ_* also increases with N for adjoint fermions.

ACKNOWLEDGMENTS

The numerical calculations presented in this work have been performed on the BlueC supercomputer at Swansea University, on a Beowulf cluster partly funded by the Royal Society and on the Horseshoe5 cluster at the supercomputing facility at the University of Southern Denmark (SDU) funded by a grant of the Danish Centre for Scientific Computing for the project ''Origin of Mass'' 2008/2009. We thank C. Allton, J. Cardy, F. Knechtli, C. McNeile, M. Piai, and F. Sannino for useful and fruitful discussions about various aspects related to this paper. We thank the organizers and participants of the workshop ''Universe in a Box,'' Lorentz Center, Leiden, NL, where some results contained in this paper were first presented and discussed. A. P. thanks the groups at CERN, Columbia University, Maryland University, Colorado University, Washington University, LLNL, SLAC, and Syracuse University for warmly hosting him and for useful and stimulating discussions about several aspects of this work. Our work has been partially supported by STFC under Contracts No. PP/E007228/1 and No. ST/G000506/1. B. L. is supported by the Royal Society, and A. P. is supported by STFC. A. R. thanks the Deutsche Forschungsgemeinschaft for financial support.

[1] S. Weinberg, Phys. Rev. D **13**, 974 (1976).
[2] L. Susskind, Phys. Rev. D **20**, 2619 (1979).
[3] B. Holdom, Phys. Lett. **150B**, 301 (1985).
[4] K. Yamawaki, M. Bando, and K.-i. Matumoto, Phys. Rev. Lett. **56**, 1335 (1986).
[5] T. Akiba and T. Yanagida, Phys. Lett. **169B**, 432 (1986).
[6] T. W. Appelquist, D. Karabali, and L. C. R. Wijewardhana, Phys. Rev. Lett. **57**, 957 (1986).
[7] W. E. Caswell, Phys. Rev. Lett. **33**, 244 (1974).
[8] T. Banks and A. Zaks, Nucl. Phys. **B196**, 189 (1982).
[9] F. Sannino and K. Tuominen, Phys. Rev. D **71**, 051901 (2005).
[10] D. D. Dietrich and F. Sannino, Phys. Rev. D **75**, 085018 (2007).
[11] M. E. Peskin and T. Takeuchi, Phys. Rev. D **46**, 381 (1992).
[12] C. T. Hill and E. H. Simmons, Phys. Rep. **381**, 235 (2003).
[13] K. Lane, arXiv:hep-ph/0202255.

[14] F. Sannino, arXiv:0804.0182.
[15] F. Sannino, arXiv:0911.0931.
[16] M. Piai, arXiv:1004.0176.
[17] C. Nunez, I. Papadimitriou, and M. Piai, Int. J. Mod. Phys. A **25**, 2837 (2010).
[18] S. Catterall and F. Sannino, Phys. Rev. D **76**, 034504 (2007).
[19] L. Del Debbio, A. Patella, and C. Pica, Phys. Rev. D **81**, 094503 (2010).
[20] S. Catterall, J. Giedt, F. Sannino, and J. Schneible, J. High Energy Phys. 11 (2008) 009.
[21] A. J. Hietanen, J. Rantaharju, K. Rummukainen, and K. Tuominen, J. High Energy Phys. 05 (2009) 025.
[22] C. Pica, L. Del Debbio, B. Lucini, A. Patella, and A. Rago, arXiv:0909.3178.
[23] S. Catterall, J. Giedt, F. Sannino, and J. Schneible, arXiv;0910.4387.
[24] T. DeGrand, Y. Shamir, and B. Svetitsky, Phys. Rev. D **79**, 034501 (2009).
[25] Y. Shamir, B. Svetitsky, and T. DeGrand, Phys. Rev. D **78**, 031502 (2008).
[26] B. Svetitsky, Nucl. Phys. **A827**, 547c (2009).
[27] A. J. Hietanen, K. Rummukainen, and K. Tuominen, Phys. Rev. D **80**, 094504 (2009).
[28] A. Hietanen, J. Rantaharju, K. Rummukainen, and K. Tuominen, Nucl. Phys. **A820**, 191c (2009).
[29] F. Bursa, L. Del Debbio, L. Keegan, C. Pica, and T. Pickup, Phys. Rev. D **81**, 014505 (2010).
[30] F. Bursa, L. Del Debbio, L. Keegan, C. Pica, and T. Pickup, arXiv:0910.2562.
[31] T. DeGrand, Phys. Rev. D **80**, 114507 (2009).
[32] T. DeGrand and A. Hasenfratz, Phys. Rev. D **80**, 034506 (2009).
[33] T. DeGrand, arXiv:0906.4543.
[34] B. Lucini, arXiv:0911.0020.
[35] Z. Fodor, K. Holland, J. Kuti, D. Nogradi, and C. Schroeder, J. High Energy Phys. 11 (2009) 103.
[36] J. B. Kogut and D. K. Sinclair, Phys. Rev. D **81**, 114507 (2010).
[37] D. K. Sinclair and J. B. Kogut, arXiv:0909.2019.
[38] T. Appelquist, G. T. Fleming, and E. T. Neil, Phys. Rev. Lett. **100**, 171607 (2008).
[39] A. Deuzeman, M. P. Lombardo, and E. Pallante, Phys. Lett. B **670**, 41 (2008).
[40] T. Appelquist, G. T. Fleming, and E. T. Neil, Phys. Rev. D **79**, 076010 (2009).
[41] E. Bilgici *et al.*, Phys. Rev. D **80**, 034507 (2009).
[42] A. Deuzeman, M. P. Lombardo, and E. Pallante, arXiv:0904.4662.
[43] Z. Fodor, K. Holland, J. Kuti, D. Nogradi, and C. Schroeder, Phys. Lett. B **681**, 353 (2009).
[44] Z. Fodor, K. Holland, J. Kuti, D. Nogradi, and C. Schroeder, arXiv:0911.2934.
[45] A. Hasenfratz, Phys. Rev. D **80**, 034505 (2009).
[46] A. Hasenfratz, arXiv:0911.0646.
[47] X.-Y. Jin and R. D. Mawhinney, Proc. Sci., LAT2009 (2009) 049 [arXiv:0910.3216].
[48] T. Appelquist *et al.*, Phys. Rev. Lett. **104**, 071601 (2010).
[49] A. Hasenfratz, arXiv:1004.1004 [Phys. Rev. D (to be published)].
[50] L. Del Debbio, M. T. Frandsen, H. Panagopoulos, and F. Sannino, J. High Energy Phys. 06 (2008) 007.
[51] G. T. Fleming, Proc. Sci., LATTICE2008 (2008) 021 [arXiv:0812.2035].
[52] E. Pallante, arXiv:0912.5188.
[53] E. Poppitz and M. Unsal, J. High Energy Phys. 09 (2009) 050.
[54] A. Armoni, Nucl. Phys. **B826**, 328 (2010).
[55] F. Sannino, Nucl. Phys. **B830**, 179 (2010).
[56] E. Poppitz and M. Unsal, J. High Energy Phys. 12 (2009) 011.
[57] L. Del Debbio, B. Lucini, A. Patella, C. Pica, and A. Rago, Phys. Rev. D **80**, 074507 (2009).
[58] L. Del Debbio, B. Lucini, A. Patella, C. Pica, and A. Rago, preceding Article, Phys. Rev. D **82**, 014509 (2010).
[59] G. Moraitis, Phys. Lett. B **690**, 96 (2010).
[60] J. C. Myers and M. C. Ogilvie, J. High Energy Phys. 07 (2009) 095.
[61] G. Cossu and M. D'Elia, J. High Energy Phys. 07 (2009) 048.
[62] O. Machtey and B. Svetitsky, Phys. Rev. D **81**, 014501 (2010).
[63] J. B. Kogut, J. Polonyi, H. W. Wyld, and D. K. Sinclair, Phys. Rev. Lett. **54**, 1475 (1985).
[64] F. Karsch and M. Lutgemeier, Nucl. Phys. **B550**, 449 (1999).
[65] J. L. Cardy, *Scaling and Renormalization in Statistical Physics* (Cambridge University Press, Cambridge, England, 1996).
[66] P. Weisz, Nucl. Phys. **B212**, 1 (1983).
[67] V. A. Miransky, Phys. Rev. D **59**, 105003 (1999).
[68] V. A. Miransky, arXiv:1004.2071.
[69] M. A. Clark and A. D. Kennedy, Phys. Rev. Lett. **98**, 051601 (2007).
[70] P. Kovtun, M. Unsal, and L. G. Yaffe, J. High Energy Phys. 06 (2007) 019.
[71] R. Narayanan and H. Neuberger, Proc. Sci., LAT2007 (2007) 020 [arXiv:0710.0098].
[72] T. J. Hollowood and J. C. Myers, J. High Energy Phys. 11 (2009) 008.
[73] P. de Forcrand, G. Schierholz, H. Schneider, and M. Teper, Phys. Lett. **160B**, 137 (1985).
[74] B. Lucini and M. Teper, Phys. Rev. D **64**, 105019 (2001).
[75] S. Necco and R. Sommer, Nucl. Phys. **B622**, 328 (2002).
[76] M. Luscher and P. Weisz, J. High Energy Phys. 07 (2002) 049.
[77] M. Caselle, M. Pepe, and A. Rago, J. High Energy Phys. 10 (2004) 005.
[78] O. Aharony and E. Karzbrun, J. High Energy Phys. 06 (2009) 012.
[79] B. Lucini, M. Teper, and U. Wenger, J. High Energy Phys. 06 (2004) 012.
[80] B. Lucini, Few-Body Syst. **36**, 161 (2005).
[81] B. Bolder *et al.*, Phys. Rev. D **63**, 074504 (2001).
[82] A. Hasenfratz and F. Knechtli, Phys. Rev. D **64**, 034504 (2001).
[83] G. T. Fleming, S. D. Cohen, H.-W. Lin, and V. Pereyra, Phys. Rev. D **80**, 074506 (2009).
[84] R. Sommer, Nucl. Phys. **B411**, 839 (1994).
[85] B. Berg and A. Billoire, Nucl. Phys. **B221**, 109 (1983).
[86] N. Evans and F. Sannino, arXiv:hep-ph/0512080.